

Large-field behavior of the LoSurdo-Stark resonances in atomic hydrogen

Gabriel Alvarez

Departamento de Física Teórica, Facultad de Ciencias Físicas, Universidad Complutense, 28040 Madrid, Spain

Harris J. Silverstone

Department of Chemistry, The Johns Hopkins University, Baltimore, Maryland 21218

(Received 10 March 1994)

The Schrödinger equation for atomic hydrogen in a large electric field F is solved by separation in parabolic coordinates. As $F \rightarrow \infty$, the scaled field f that enters the separated equations tends to 0. Thus the large- F asymptotics depend on the small- f behavior of the separated equations, each of which in turn is equivalent to a quartically perturbed two-dimensional anharmonic oscillator. The Bender-Wu branch cuts of the oscillator play a major role in the hydrogen asymptotics. A simple iterative algorithm permits the calculation of the branch points, at which two eigenvalues coincide. We have found numerically that, as $F \rightarrow \infty$, the separation constant β_1 returns to the smaller of the unperturbed values $\beta_1^{(0)}$ or $\beta_2^{(0)}$. At the same time, β_2 tends to the negative of the smaller value. As the real electric field F increases from 0 to ∞ , in each case that $\beta_1^{(0)}$ and $\beta_2^{(0)}$ are not equal, the trajectory of either f or $e^{-i\pi}f$ (but not both) loops around a single branch point and passes through the cut that joins the two ($\beta_1^{(0)}$ and $\beta_2^{(0)}$) Riemann triple sheets. All other branch cuts are avoided. No branch cuts are crossed if $\beta_1^{(0)} = \beta_2^{(0)}$. The known small- f asymptotic expansion for the discontinuity of the separation constant in the f plane across the negative real axis leads to the large- F asymptotic expansion for E in terms of the parabolic quantum numbers n_1 , n_2 , and m .

PACS number(s): 32.60.+i

I. INTRODUCTION

Although atomic hydrogen in an external electric field was first studied experimentally in 1913 by LoSurdo [1] and Stark [2] and quantum mechanically in 1926 by Schrödinger [3], still the LoSurdo-Stark effect continues to attract both experimental and theoretical interest. Starting in 1978, modern beam and laser techniques were applied by Koch [4] to measure energy shifts and ionization rates, while at the same time there was a revival of theoretical interest that involved numerical integration [5–9], perturbation theory [10], complex variational calculations [11,12], semiclassical methods [13–15], and the proof that the perturbation expansions were divergent, but Borel summable to the complex resonance eigenvalues [16]. Most recently, photoionization cross sections of various states have been measured in fields up to several kV/cm [17–19], and in one instance, a few MV/cm [20]. The theoretical explanation of these experiments can be based on variational calculations of the complex resonance eigenvalues and complex transition moments [21,22]. Such techniques have been extended to larger atoms and molecules [23]. The general consensus is that hydrogen is understood experimentally and theoretically both at low static electric fields—the perturbative region—where the energy levels shift and split, and at high fields where there is also ionization.

Experimentally accessible fields in practice have been less than 0.001 a.u., or $\sim 5 \times 10^6$ V/cm. In 1979, Benassi, Grecchi, Harrell, and Simon [24] and Benassi and Grecchi [25] determined the high-field asymptotics of a resonance thought to come from the ground state and

of the first two excited states [25]. It was clear, however, that the lowest field for which the asymptotic formula was valid was many orders of magnitude higher than any field used in prior numerical calculations. Benassi and Grecchi [25], by using the separability of the LoSurdo-Stark Schrödinger equation in parabolic coordinates, pushed the complex variational method to fields as high as 10^{22} a.u. This touched upon the asymptotic regime and also permitted preliminary numerical exploration of the connection with the asymptotics of the anharmonic oscillator—the separated equations are equivalent to an anharmonic oscillator, and Bender and Wu [26] had established that the complex anharmonic oscillator eigenvalues are all analytic continuations of each other with respect to the complex anharmonicity constant. Benassi and Grecchi plotted the complex trajectory of the coupling constant for the ground and one excited state and conjectured the position of the Bender-Wu branch cuts, one of which had to be crossed for the asymptotic formula for the excited state to be valid. Thus two interesting topics that required still higher fields were identified, but not thoroughly studied: the asymptotics of the resonance eigenvalues and the Bender-Wu phenomenology of the separation constants.

In previous work on photoionization [21,22] we developed a computer program to calculate LoSurdo-Stark resonances for any set of quantum numbers and for any field. Although intended for laboratory fields, the program works for fields that are orders of magnitude higher—for instance, 10^{48} a.u.—high enough to answer the questions raised by the work of Benassi, Grecchi, Harrell, and Simon [24]. We obtain in this paper analytical and nu-

merical results on LoSurdo-Stark resonances at extremely high fields. In particular, (i) we fix the value of a parameter [25] in the second term of the asymptotic formula for $\arg E$, which in turn permits generation of the rest of the expansion for $\arg E$ and for $|E|$; (ii) we present an algorithm to calculate the position of the Bender-Wu branch points to high accuracy (originally the branch points had only been approximated by semiclassical methods [26], later by matrix methods applied to a simpler related problem [27], and still later by numerical integration of the Schrödinger equation [28]); (iii) we determine how the trajectory of the complex anharmonicity constant in the separated equations passes through Bender-Wu branch cuts; (iv) we describe the topology of the Riemann surface, which is more intricate than conjectured by Bender and Wu: not only are the sheets belonging to perturbed adjacent harmonic oscillator eigenvalues n and $n+1$ connected by a pair of branch cuts, but the sheets of *any pair* of eigenvalues are connected by two branch cuts. There are a few additional points that include, for instance, the Herglotz property. In short, we give a complete picture of each resonance eigenvalue, from zero to infinite field.

II. SEPARATION OF VARIABLES

We briefly review some equations basic to the solution of the LoSurdo-Stark Schrödinger equation, in part to fix notation.

A. Parabolic coordinates

The Schrödinger equation for a hydrogenic atom of nuclear charge Z in a uniform external electric field F directed along the z axis,

$$\left(-\frac{1}{2}\Delta - \frac{Z}{r} + Fz\right)\Psi = E\Psi, \quad (1)$$

separates in parabolic coordinates

$$\begin{aligned} x &= \sqrt{\xi\eta} \cos \phi, \\ y &= \sqrt{\xi\eta} \sin \phi, \\ z &= \frac{1}{2}(\xi - \eta). \end{aligned} \quad (2)$$

We seek solutions in the form

$$\Psi(\xi, \eta, \phi) = \frac{\phi_1(\xi)\phi_2(\eta)}{\xi^{1/2}\eta^{1/2}} \frac{1}{\sqrt{2\pi}} e^{im\phi} \quad (m = 0, \pm 1, \pm 2, \dots), \quad (3)$$

for which the Schrödinger equation reduces to the two one-dimensional equations

$$H(-2E, F/4)\phi_1(s) = \beta_1(-2E, F/4)\phi_1(s), \quad (4)$$

$$H(-2E, -F/4)\phi_2(s) = \beta_2(-2E, -F/4)\phi_2(s), \quad (5)$$

where

$$H(k, g) = -s \frac{d^2}{ds^2} + \frac{m^2 - 1}{4s} + \frac{k}{4}s + gs^2 \quad (6)$$

and the separation constants β_1 and β_2 are coupled by

$$\beta_1(-2E, F/4) + \beta_2(-2E, -F/4) = Z. \quad (7)$$

Since the operator $H(k, g)$ does not depend on the sign of m , we simplify the notation hereafter with the convention that $m \geq 0$. [$H(k, g)$ is transformationally equivalent to a two-dimensional anharmonic oscillator with force constant k and quartic anharmonicity constant $2g$. See Sec. II E.]

B. Symanzik scaling

The separated Eqs. (4) and (5) are particular cases of the generic

$$H(k, g)\phi(s) = \beta(k, g)\phi(s). \quad (8)$$

An important property of Eq. (8), usually known as Symanzik scaling [29], follows from the change of variable $s \rightarrow \lambda s$:

$$\lambda^{-1}\beta(\lambda^2 k, \lambda^3 g) = \beta(k, g). \quad (9)$$

In particular, one can scale out either k or g in the sense that

$$\beta(k, g) = k^{1/2}\beta(1, k^{-3/2}g) \quad (10)$$

$$= g^{1/3}\beta(g^{-2/3}k, 1). \quad (11)$$

Note that the $\beta_1(f)$ and $\beta_2(f)$ of Ref. [22] correspond to $\beta(1, f)$ and $\beta(1, e^{-i\pi}f)$ here, where

$$f = \frac{1}{4}(-2E)^{-3/2}F \quad (12)$$

and

$$E = -\frac{1}{2}[\beta_1(f) + \beta_2(f)]^{-2}. \quad (13)$$

C. Eigenvalues and eigenfunctions of $H(1, 0)$

Let us first consider the ‘‘unperturbed eigenvalue problem’’ $H(1, 0)\phi = \beta(1, 0)\phi$. The boundary conditions are that $s^{-1/2}\phi(s)$ be bounded everywhere and that $\phi(s)$ be square integrable on $[0, \infty)$ with respect to the volume element $s^{-1}ds$. The differential equation reduces to

$$\left(-s \frac{d^2}{ds^2} + \frac{m^2 - 1}{4s} + \frac{1}{4}s\right)\phi_{n,m}(s) = \beta_{n,m}\phi_{n,m}(s). \quad (14)$$

As is well known, the solutions are

$$\phi_{n,m}(s) = \left(\frac{n!}{(n+m)!}\right)^{1/2} s^{(m+1)/2} e^{-s/2} I_n^{(m)}(s), \quad (15)$$

where

$$\beta_{n,m} = n + (m + 1)/2, \quad (16)$$

$n = 0, 1, 2, \dots$, and $L_n^{(m)}(s)$ are the associated Laguerre polynomials [30]. These eigenfunctions are orthonormal with respect to the $s^{-1} ds$ volume element

$$\int_0^\infty \phi_{n_1, m_1}(s) \phi_{n_2, m_2}(s) s^{-1} ds = \delta_{n_1, n_2} \delta_{m_1, m_2}. \quad (17)$$

[Recall our convention that $m \geq 0$; otherwise m on the right-hand sides of Eqs. (15) and (16) would have to be replaced by $|m|$.]

The implicit Eq. (7), with $F = 0$, and with Eq. (10) to scale out the energy term $k = -2E$, turns out to be

$$\left(n_1 + \frac{m+1}{2}\right) \sqrt{-2E} + \left(n_2 + \frac{m+1}{2}\right) \sqrt{-2E} = Z, \quad (18)$$

from which the familiar formula for the eigenvalues of the hydrogenic atom follows:

$$E = -\frac{Z^2}{2(n_1 + n_2 + m + 1)^2}. \quad (19)$$

D. Resonance solutions

When $g \neq 0$, the differential equation

$$\left(-s \frac{d^2}{ds^2} + \frac{m^2 - 1}{4s} + \frac{k}{4}s + gs^2\right) \phi_{n,m}(s) = \beta_{n,m} \phi_{n,m}(s) \quad (20)$$

has a unique (up to a multiplicative constant) solution dominated by the asymptotic behavior

$$\phi(s) \sim \exp\left(-\frac{2}{3}g^{1/2}s^{3/2}\right) \quad (21)$$

that tends to zero as $s \rightarrow \infty$ in the sector

$$\left|\frac{3}{2} \arg s + \frac{1}{2} \arg g\right| < \frac{\pi}{2}. \quad (22)$$

The resonance solutions of Eq. (20) are those solutions that satisfy simultaneously the boundary conditions at the origin and those at ∞ given by Eqs. (21) and (22). The corresponding values of the parameter β are called resonance eigenvalues.

The LoSurdo-Stark resonance energies are those values of the parameter E for which the resonance eigenvalues of the separated equations (4) and (5) satisfy the implicit equation (7). The numerical calculation of the resonance eigenvalues and eigenvectors of both the separated Eqs. (4) and (5) and the solution of the implicit Eq. (7) for the LoSurdo-Stark resonances have been discussed in detail in Ref. [22]. The main idea is to expand the resonance wave function as a linear combination of square-integrable basis functions along a ray lying halfway in the

sector of convergence given by Eq. (22). Technical details can be found in Ref. [22], and the calculation should be considered as automatic for purposes of this paper.

It can be shown [14,31] that the definition of resonance given here is equivalent to the usual operator-theoretic definitions. Furthermore, Graffi, Grecchi, and Simon [32] proved that every LoSurdo-Stark resonance wave function can be written in parabolic coordinates as a separated product or as a finite linear combination of products; i.e., there are no other resonances than the solutions of Eq. (7).

The relation between the mathematical concept of resonance and physical observables (in particular the photoionization cross section of atomic hydrogen in an electric field) has been discussed in Ref. [22].

E. Relation to the two-dimensional isotropic anharmonic oscillator

We close this section with the explicit connection between the two-dimensional isotropic anharmonic oscillator and the separated equations (4) and (5). The two-dimensional isotropic anharmonic oscillator with harmonic force constant k and quartic coupling constant $2g$ has the Schrödinger equation

$$\left[-\frac{1}{2}\Delta + \frac{k}{2}(x^2 + y^2) + 2g(x^2 + y^2)^2\right] \Psi = 2\beta\Psi. \quad (23)$$

With the substitutions,

$$x = \sqrt{s} \cos \theta, \quad (24)$$

$$y = \sqrt{s} \sin \theta, \quad (25)$$

$$\Psi(s, \theta) = s^{-1/2} \phi(s) \frac{1}{\sqrt{2\pi}} e^{im\theta} \quad (m = 0, \pm 1, \pm 2, \dots), \quad (26)$$

one finds that $\phi(s)$ must satisfy precisely Eq. (8).

III. BENDER-WU BRANCH POINTS

At large F , theoretical arguments by Herbst [31] as well as numerical calculations indicate that for any resonance, both $\text{Re } E$ and $-\text{Im } E$ tend to ∞ , consistent with the asymptotic phase $-\pi/3$ and magnitude $2^{-5/3}(F \ln F)^{2/3}$ of Benassi and Grecchi [25]. The implication for the asymptotic magnitude of f from Eq. (12) is that $f = O(1/\ln F)$ as $F \rightarrow \infty$. This has two interesting consequences: the first is that as $F \rightarrow \infty$, $f s^2$ becomes again a small perturbation, and the second, which follows from Eq. (13), is that at $F = \infty$, $\beta_1 = -\beta_2$. That is, one separation constant comes back to an unperturbed eigenvalue, and the other to the negative of the same unperturbed eigenvalue. But how? The answer must be sought in the path f traces in the complex plane, crossing Bender-Wu branch cuts.

Analytic continuation of the anharmonic oscillator eigenvalues was first studied by Bender and Wu [26] in the JWKB approximation and then rigorously by Simon [29]. The picture they developed is that $\beta(1, f)$ has a cube-root “global branch point” at the origin that is a limit point of sequences of square-root branch points with asymptotic phases $\arg f = 3\pi/2$ and $\arg f = 9\pi/2$. At each square-root branch point two levels coincide. [The word “cross” is usually used, but “coincide” may be more appropriate. (See Sec. III D.) We use both terms interchangeably.] Initially Bender and Wu thought that only adjacent levels cross. That is, start with $\beta(1, f)$ a particular anharmonic oscillator eigenvalue, say the n th, with f positive; follow a path that encircles only one branch point and return to the starting point; then $\beta(1, f)$ is equal to either the $(n - 1)$ th or $(n + 1)$ th anharmonic oscillator eigenvalue. To get from one eigenvalue to a nonadjacent one, Bender and Wu suggested that the coupling constant has to “cascade” through a sequence of branch cuts. After numerical calculations of Bender-Wu branch points for the potential $\epsilon|x| + x^2$, Bender, Happ, and Svetitsky [27] recognized that nonadjacent levels could be directly connected, but they did not fix a classification scheme to assign branch points to pairs of unperturbed eigenvalues. Shanley [28] later numerically integrated the Schrödinger equation to find a large number of Bender-Wu branch points for the original anharmonic oscillator problem, many of which agreed well with the JWKB calculations of Bender and Wu [26], but which disagreed in the assignment of which levels were crossing. We shall see below that the original and evolving picture of the singularities requires a slight modification.

To understand what happens to $\beta(1, f)$, $\beta(1, e^{-\pi i} f)$, and $E(F)$ as f traverses the path generated by the implicit Eqs. (7) and (12) with F increasing from 0 to ∞ , it is necessary to know *accurately* the location of the Bender-Wu branch points. We describe here how to calculate numerically the branch points from the Schrödinger equation, variationally.

A. Numerical calculation of Bender-Wu branch points

The variational program developed in Ref. [22] is able to calculate anharmonic oscillator eigenvalues for any value of f . By definition, a Bender-Wu branch point occurs when two anharmonic oscillator eigenvalues cross. Suppose a crossing point occurs at f_c . Denote by $\beta_+(1, f)$ and $\beta_-(1, f)$ the two levels that cross. Since the f_c is a square-root branch point, $\beta_+(1, f)$ and $\beta_-(1, f)$ are the two branches of a Puiseux series in a neighborhood of f_c :

$$\beta_{\pm}(1, f) = \beta(1, f_c) \pm a_{1/2}(f - f_c)^{1/2} + \dots \quad (27)$$

Pick two initial values f_1 and f_2 close to the branch point f_c , and note that

$$\sqrt{Q_2} \equiv \frac{\beta_+(1, f_1) - \beta_-(1, f_1)}{\beta_+(1, f_2) - \beta_-(1, f_2)} \approx \frac{(f_1 - f_c)^{1/2}}{(f_2 - f_c)^{1/2}}. \quad (28)$$

Solving this for f_c , one finds

$$f_c \approx \frac{f_1 - f_2 Q_2}{1 - Q_2}. \quad (29)$$

This equation suggests the following iterative algorithm to be used with the anharmonic oscillator eigenvalue program: For $i = 1, 2, \dots$,

$$Q_{i+1} = \left[\frac{\beta_+(1, f_i) - \beta_-(1, f_i)}{\beta_+(1, f_{i+1}) - \beta_-(1, f_{i+1})} \right]^2, \quad (30)$$

$$f_{i+2} = \frac{f_i - f_{i+1} Q_{i+1}}{1 - Q_{i+1}}. \quad (31)$$

As a computational procedure, this converged without difficulty in typically ten iterations. Some illustrative branch points, calculated with extended precision, are presented in columns 4 and 5 of Tables I and II. All figures given are accurate. The $m = 0$ branch points are plotted in Fig. 1. Note the strongly regular pattern for the plot of the reciprocals $1/f_c$ in Fig. 1(b).

B. Identification and labeling of Bender-Wu branch points; triple sheets T_n

What do not come out of this algorithm are the quantum-number assignments n_1 and n_2 given in columns 2 and 3 of Tables I and II. Their identification is more subtle. That the branch points can be labeled by pairs of quantum numbers is a statement in itself about the topology of the Riemann surface for $\beta(1, f)$.

Recall that the origin is a cubic-root global branch point, which is a consequence of Symanzik scaling [Eq. (9)],

$$\beta(1, e^{i6\pi} f) = \beta(1, f). \quad (32)$$

The primary unit of the Riemann surface for $\beta(1, f)$ is thus a triple sheet. To each unperturbed harmonic oscillator quantum number n one can assign a triple sheet T_n . On T_n , $\beta(1, 0) = n + (m + 1)/2$. The value of $\beta(1, |f|e^{i\theta})$ is obtained by continuity on following the path from 0 to $|f|$ on the positive real axis and then from $|f|$ to $|f|e^{i\theta}$ on the triple circle of radius $|f|$. This recipe is unambiguous for all f except for those at which there is a Bender-Wu branch point somewhere on the triple circle of radius $|f|$.

Suppose now that we have a particular branch point f_c , the assignment of which is to be determined. We follow $\beta(1, f)$ numerically along a path on the positive real axis from the origin to $|f_c| - \epsilon$, then along an arc from $|f_c| - \epsilon$ to $(|f_c| - \epsilon)e^{i\theta_c}$, where $\theta_c = \arg f_c$, then along a circle of radius ϵ centered about f_c , and then backwards from $(|f_c| - \epsilon)e^{i\theta_c}$ to $|f_c| - \epsilon$ to the origin. The ϵ should be sufficiently small that only one branch point f_c is trapped, and no others. To be sure that the path

TABLE I. Bender-Wu branch points $f_{n_1 n_2}^{(3)}$ of $\beta(1, f)$, in the third quadrant of the first Riemann sheet, and corresponding values of $\beta(1, f)$, for $m = 0$ and $0 \leq n_1 < n_2 \leq 10$.

| m | n_1 | n_2 | $ f_{n_1 n_2}^{(3)} $ | $\arg f_{n_1 n_2}^{(3)}$ | $\text{Re } \beta(1, f_{n_1 n_2}^{(3)})$ | $-\text{Im } \beta(1, f_{n_1 n_2}^{(3)})$ |
|-----|-------|-------|-------------------------|--------------------------|--|---|
| 0 | 0 | 1 | 0.018 838 404 078 069 6 | 3.804 652 181 161 366 1 | 0.574 115 148 1 | 0.056 414 245 0 |
| 0 | 0 | 2 | 0.011 654 854 413 201 8 | 4.144 916 165 936 529 0 | 0.585 851 707 6 | 0.035 619 684 9 |
| 0 | 0 | 3 | 0.008 254 472 554 437 9 | 4.297 737 896 767 240 5 | 0.585 992 299 1 | 0.025 107 614 5 |
| 0 | 0 | 4 | 0.006 351 438 586 740 8 | 4.384 166 233 315 551 3 | 0.584 384 932 1 | 0.019 178 415 0 |
| 0 | 0 | 5 | 0.005 149 260 732 693 3 | 4.439 837 535 198 390 0 | 0.582 585 838 8 | 0.015 439 468 5 |
| 0 | 0 | 6 | 0.004 324 879 138 921 3 | 4.478 774 813 990 515 0 | 0.580 908 521 2 | 0.012 886 134 9 |
| 0 | 0 | 7 | 0.003 725 778 570 199 3 | 4.507 592 760 801 044 5 | 0.579 407 171 6 | 0.011 039 236 9 |
| 0 | 0 | 8 | 0.003 271 299 256 666 1 | 4.529 817 891 994 735 2 | 0.578 073 938 8 | 0.009 644 676 6 |
| 0 | 0 | 9 | 0.002 914 990 213 112 6 | 4.547 503 400 692 902 7 | 0.576 887 426 0 | 0.008 556 173 8 |
| 0 | 0 | 10 | 0.002 628 286 312 592 7 | 4.561 926 733 018 193 9 | 0.57 582 569 26 | 0.007 683 927 4 |
| 0 | 1 | 2 | 0.009 687 394 774 852 6 | 3.506 153 420 738 782 4 | 1.455 291 723 3 | 0.116 219 783 4 |
| 0 | 1 | 3 | 0.007 627 521 743 206 0 | 3.799 435 815 117 423 9 | 1.517 197 521 9 | 0.110 223 992 9 |
| 0 | 1 | 4 | 0.006 141 760 289 004 2 | 3.977 834 848 335 285 8 | 1.545 604 174 7 | 0.094 419 410 5 |
| 0 | 1 | 5 | 0.005 090 880 195 331 5 | 4.097 094 047 859 972 2 | 1.559 987 768 4 | 0.080 523 998 7 |
| 0 | 1 | 6 | 0.004 326 549 594 125 3 | 4.182 223 626 349 916 0 | 1.567 827 816 6 | 0.069 486 198 2 |
| 0 | 1 | 7 | 0.003 752 004 876 536 8 | 4.245 998 644 483 719 3 | 1.572 313 394 5 | 0.060 798 404 2 |
| 0 | 1 | 8 | 0.003 307 032 762 872 3 | 4.295 565 652 669 192 9 | 1.574 947 322 6 | 0.053 883 134 8 |
| 0 | 1 | 9 | 0.002 953 502 040 562 8 | 4.335 214 713 921 349 1 | 1.576 498 867 8 | 0.048 291 087 2 |
| 0 | 1 | 10 | 0.002 666 503 044 380 0 | 4.367 669 997 950 496 2 | 1.577 389 029 0 | 0.043 696 534 3 |
| 0 | 2 | 3 | 0.006 439 801 016 267 0 | 3.396 402 435 786 417 6 | 2.307 255 295 4 | 0.155 221 528 6 |
| 0 | 2 | 4 | 0.005 543 519 181 765 5 | 3.633 607 197 384 533 4 | 2.401 203 022 0 | 0.176 273 371 8 |
| 0 | 2 | 5 | 0.004 774 137 587 348 3 | 3.797 993 773 615 463 5 | 2.457 379 798 7 | 0.168 689 868 2 |
| 0 | 2 | 6 | 0.004 152 937 952 867 3 | 3.918 650 612 985 627 8 | 2.492 523 644 9 | 0.154 913 854 9 |
| 0 | 2 | 7 | 0.003 655 421 623 664 6 | 4.010 773 728 450 813 5 | 2.515 503 549 9 | 0.140 811 037 4 |
| 0 | 2 | 8 | 0.003 253 909 840 363 0 | 4.083 308 497 542 291 2 | 2.531 114 701 4 | 0.127 979 015 7 |
| 0 | 2 | 9 | 0.002 925 831 216 832 1 | 4.141 857 975 684 149 3 | 2.542 063 619 3 | 0.116 729 491 3 |
| 0 | 2 | 10 | 0.002 654 158 466 829 3 | 4.190 096 440 861 790 7 | 2.549 947 536 8 | 0.106 978 217 1 |
| 0 | 3 | 4 | 0.004 809 817 372 539 5 | 3.338 955 448 305 638 9 | 3.150 630 721 3 | 0.183 253 830 7 |
| 0 | 3 | 5 | 0.004 324 779 011 262 7 | 3.536 458 775 153 790 1 | 3.264 984 791 7 | 0.230 301 226 5 |
| 0 | 3 | 6 | 0.003 870 384 843 816 2 | 3.683 261 490 978 959 0 | 3.342 820 875 6 | 0.236 125 437 9 |
| 0 | 3 | 7 | 0.003 473 552 368 701 7 | 3.797 321 594 040 279 5 | 3.397 013 114 4 | 0.228 104 771 2 |
| 0 | 3 | 8 | 0.003 134 602 768 397 1 | 3.888 440 755 284 492 7 | 3.435 735 517 9 | 0.215 445 731 1 |
| 0 | 3 | 9 | 0.002 846 511 429 332 1 | 3.962 820 739 490 330 2 | 3.464 094 817 4 | 0.201 724 395 0 |
| 0 | 3 | 10 | 0.002 601 064 000 766 2 | 4.024 629 337 895 142 9 | 3.485 332 091 0 | 0.188 375 988 5 |
| 0 | 4 | 5 | 0.003 834 636 058 846 7 | 3.303 401 687 678 841 3 | 3.990 303 807 3 | 0.204 958 430 8 |
| 0 | 4 | 6 | 0.003 535 590 567 692 0 | 3.472 524 189 178 429 2 | 4.118 590 082 6 | 0.275 086 579 4 |
| 0 | 4 | 7 | 0.003 241 184 653 018 3 | 3.603 766 337 761 525 6 | 4.212 968 695 9 | 0.295 567 897 2 |
| 0 | 4 | 8 | 0.002 970 946 979 025 9 | 3.709 631 803 710 580 8 | 4.283 252 194 4 | 0.296 093 607 0 |
| 0 | 4 | 9 | 0.002 729 679 944 614 3 | 3.796 933 139 546 592 0 | 4.336 449 944 1 | 0.287 868 281 1 |
| 0 | 4 | 10 | 0.002 516 677 021 453 8 | 3.870 123 621 319 048 5 | 4.377 384 791 9 | 0.275 916 386 0 |
| 0 | 5 | 6 | 0.003 186 877 070 814 6 | 3.279 128 166 677 139 1 | 4.828 024 111 6 | 0.222 602 598 9 |
| 0 | 5 | 7 | 0.002 985 950 572 029 7 | 3.427 153 724 007 983 6 | 4.966 394 850 6 | 0.313 036 157 8 |
| 0 | 5 | 8 | 0.002 782 013 065 341 9 | 3.545 403 330 638 220 6 | 5.073 609 994 8 | 0.347 958 349 9 |
| 0 | 5 | 9 | 0.002 588 460 363 475 8 | 3.643 327 462 661 032 6 | 5.157 244 502 4 | 0.358 200 033 8 |
| 0 | 5 | 10 | 0.002 410 125 810 747 4 | 3.725 974 936 721 648 1 | 5.223 191 944 8 | 0.356 142 637 8 |
| 0 | 6 | 7 | 0.002 725 741 499 531 6 | 3.261 449 787 648 277 9 | 5.664 578 477 1 | 0.237 436 080 0 |
| 0 | 6 | 8 | 0.002 582 294 679 413 9 | 3.393 218 709 835 377 5 | 5.810 583 817 9 | 0.345 837 674 2 |
| 0 | 6 | 9 | 0.002 433 787 138 706 2 | 3.500 691 861 448 576 5 | 5.927 981 287 3 | 0.394 475 976 0 |
| 0 | 6 | 10 | 0.002 289 506 949 738 9 | 3.591 427 157 805 015 3 | 6.022 716 016 9 | 0.414 769 333 0 |
| 0 | 7 | 8 | 0.002 380 892 686 870 2 | 3.247 971 157 047 414 1 | 6.500 375 698 9 | 0.250 214 728 3 |
| 0 | 7 | 9 | 0.002 273 768 638 825 1 | 3.366 835 456 508 664 7 | 6.652 365 003 0 | 0.374 660 509 1 |
| 0 | 7 | 10 | 0.002 161 376 689 658 6 | 3.465 307 886 303 969 8 | 6.778 011 921 1 | 0.436 149 301 9 |
| 0 | 8 | 9 | 0.002 113 341 453 197 6 | 3.237 337 162 011 550 4 | 7.335 650 473 0 | 0.261 428 498 7 |
| 0 | 8 | 10 | 0.002 030 523 311 338 2 | 3.345 706 392 963 920 3 | 7.492 460 032 5 | 0.400 332 070 6 |
| 0 | 9 | 10 | 0.001 899 754 065 949 4 | 3.228 722 140 435 043 2 | 8.170 547 805 5 | 0.271 412 283 8 |

encloses precisely one single branch point, it is necessary to calculate the location of all the branch points in the region of interest. It turns out that on each triple sheet except for two, $\beta(1, f)$ starts and finishes with the same

value $\beta(1, 0) = n + (m + 1)/2$, which is characteristic of that triple sheet. But for two triple sheets, say T_{n_1} and T_{n_2} , the starting and ending values are interchanged. That is, if $\beta(1, 0) = n_1 + (m + 1)/2$ at the beginning, then

TABLE II. More Bender-Wu branch points: $|m| = 1$ and $|m| = 2$.

| m | n_1 | n_2 | $ f_{n_1, n_2}^{(3)} $ | $\arg f_{n_1, n_2}^{(3)}$ | $\text{Re } \beta(1, f_{n_1, n_2}^{(3)})$ | $-\text{Im } \beta(1, f_{n_1, n_2}^{(3)})$ |
|-----|-------|-------|-------------------------|---------------------------|---|--|
| 1 | 0 | 1 | 0.013 070 694 860 563 7 | 3.620 045 743 060 926 2 | 1.025 623 856 7 | 0.085 597 340 9 |
| 1 | 0 | 2 | 0.009 367 946 647 392 7 | 3.945 309 057 660 985 0 | 1.061 998 040 7 | 0.068 683 697 1 |
| 1 | 0 | 3 | 0.007 125 538 978 208 2 | 4.120 108 630 271 188 4 | 1.073 998 539 6 | 0.053 890 191 3 |
| 1 | 1 | 2 | 0.007 787 226 388 745 3 | 3.443 251 926 775 438 2 | 1.886 245 937 0 | 0.135 993 703 3 |
| 1 | 1 | 3 | 0.006 457 298 468 116 9 | 3.706 944 058 761 609 1 | 1.965 019 926 2 | 0.142 830 659 4 |
| 1 | 2 | 3 | 0.005 523 956 150 953 1 | 3.364 667 793 426 273 0 | 2.732 117 822 9 | 0.169 432 238 3 |
| 2 | 0 | 1 | 0.010 059 888 409 431 9 | 3.524 656 523 392 188 6 | 1.470 275 003 2 | 0.106 105 865 6 |
| 2 | 0 | 2 | 0.007 806 723 296 248 0 | 3.820 733 489 762 295 1 | 1.525 403 146 9 | 0.098 548 672 8 |
| 2 | 1 | 2 | 0.006 544 787 679 647 9 | 3.401 863 768 436 673 5 | 2.318 780 313 3 | 0.150 767 880 8 |

at the end $\beta(1, 0) = n_2 + (m + 1)/2$, and vice versa. In this way, each branch point is associated with exactly one pair of harmonic oscillator levels n_1 and n_2 , whose values are swapped between the beginning and end of the path.

By way of example, we plot in Fig. 2(a) one such path in the complex plane that encloses the branch point at

$f_c \approx -0.0060 - i0.0047$, which connects the $n = 1$ and $n = 3$ levels in the quadrant $\pi \leq \arg f \leq 3\pi/2$. (The “return” is on $|f| = |f_c| + \epsilon$, rather than on $|f| = |f_c| - \epsilon$, to permit discrimination between the outgoing and returning paths on the plot.) Other nearby branch points are indicated on the plot, and one typical branch cut

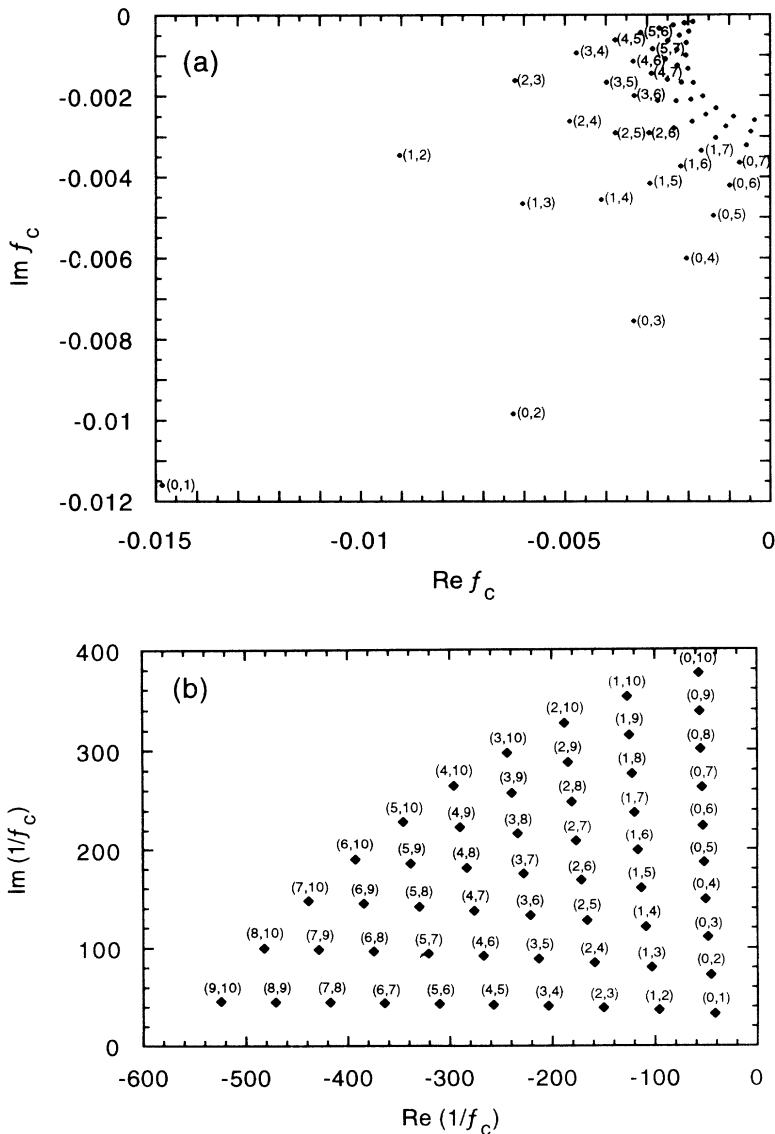


FIG. 1. $m = 0$ Bender-Wu branch points. (a) The branch points $f_{n_1, n_2}^{(3)}$ that lie in the third quadrant of the first sheet. Labels (n_1, n_2) are indicated to the right of as many branch points as permitted by clarity. (b) The same branch points as in (a), but plotted as reciprocals: $1/f_{n_1, n_2}^{(3)}$. All labels (n_1, n_2) are shown.

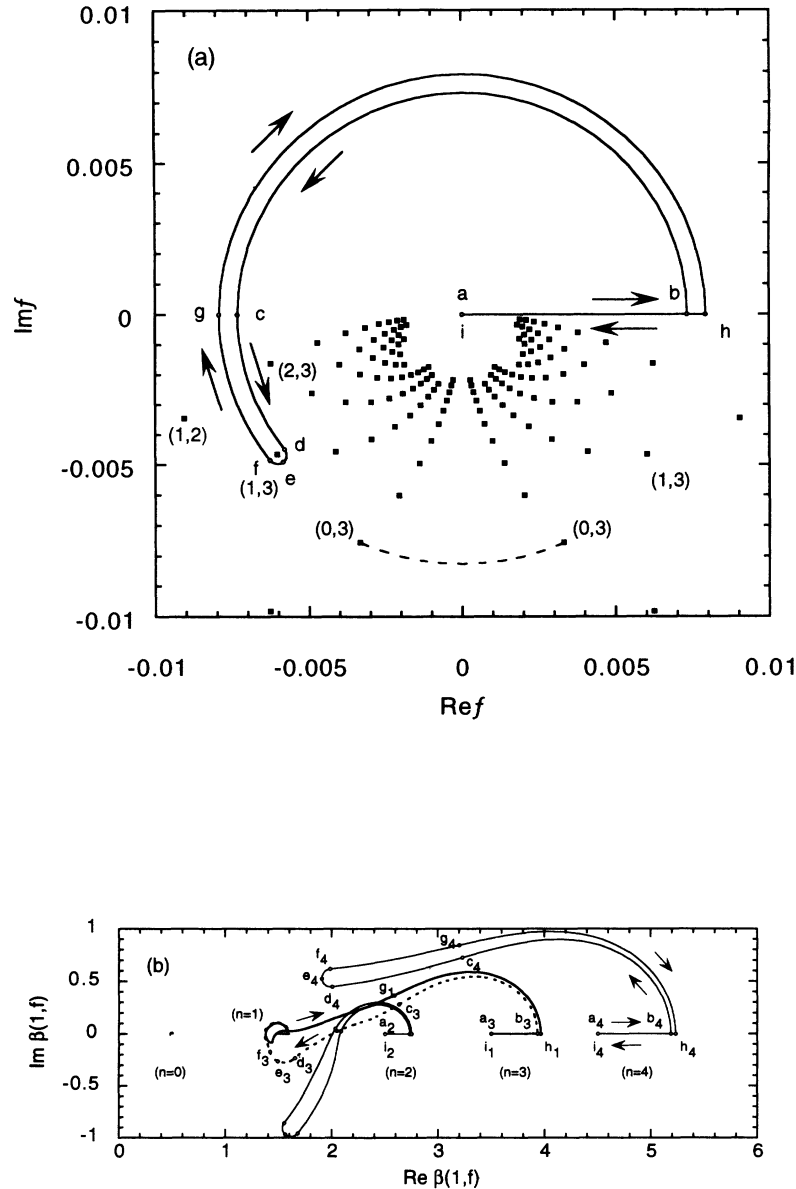


FIG. 2. Identification of the branch point $f_{13}^{(3)} = 0.0076275217432060 e^{i3.7994358151174239}$. (a) A path on the first sheet that starts out at the origin (point a), follows the real axis to $f = 0.00732\dots$ (point b), follows the arc $f = 0.00732\dots e^{i\theta}$ as θ increases from 0 through π (point c) to 3.7994358151174239 (point d), then follows a semicircle of radius 0.0003 counter-clockwise about $f_{13}^{(3)}$ (point e is at $-\pi/2$, point f at $-\pi$), and traces backwards an arc of radius $0.00792\dots$ back through π (point g) to $\theta = 0$ (point h), and the real axis back to the origin (point i). The branch points identified in Fig. 1 are shown, as well as their partners in the fourth quadrant of the first sheet, and four $[(0,3), (1,3), (2,3), \text{and } (1,2)]$ plus $(1,3)$ and $(0,3)$ in the fourth quadrant are labeled for reference. The partners in each pair define a branch cut. For illustration, the branch cut that joins $f_{03}^{(3)}$ with $f_{03}^{(4)}$ along an arc of constant $|f|$ is shown by a dashed line. (b) The trajectories of $\beta(1, f)$ that originate from the five lowest harmonic oscillator eigenvalues at $f = 0$. The images of the starting and intermediate points from some of the trajectories have been labeled with a_n, b_n, \dots, i_n . The trajectories for $n = 0, 2$, and 4 all start and return from the same points $\beta(1, 0) = n + 1/2$. The $n = 0$ trajectory is barely visible because of the scale of the plot. The trajectory that starts with $n = 1$ at $\beta(1, f) = 1.5$ (solid line) ends at $\beta(1, f) = 3.5$, while the trajectory that starts with $n = 3$ at $\beta(1, f) = 3.5$ (dashed line) ends at $\beta(1, f) = 1.5$. (c) Twofold magnification of (b) to show more clearly how the trajectory that starts at $\beta(1, f) = 1.5$ ends at $\beta(1, f) = 3.5$, and vice versa. (d) All the branch points $f_{j,N}^{(3)}$ and $f_{j,N}^{(4)}$ (for $N \leq 10$), and their corresponding cuts, on the first sheet of T_3 . The pattern seems typical for T_n in general: $|f_{j,n}^{(i)}|$ decreases monotonically as j increases; the “opening half angle” of the branch cut $3\pi/2 - \arg f_{j,n}^{(3)}$ at first increases as j increases from 0 to $n + 1$ and then decreases monotonically (perhaps to 0) as j increases further.

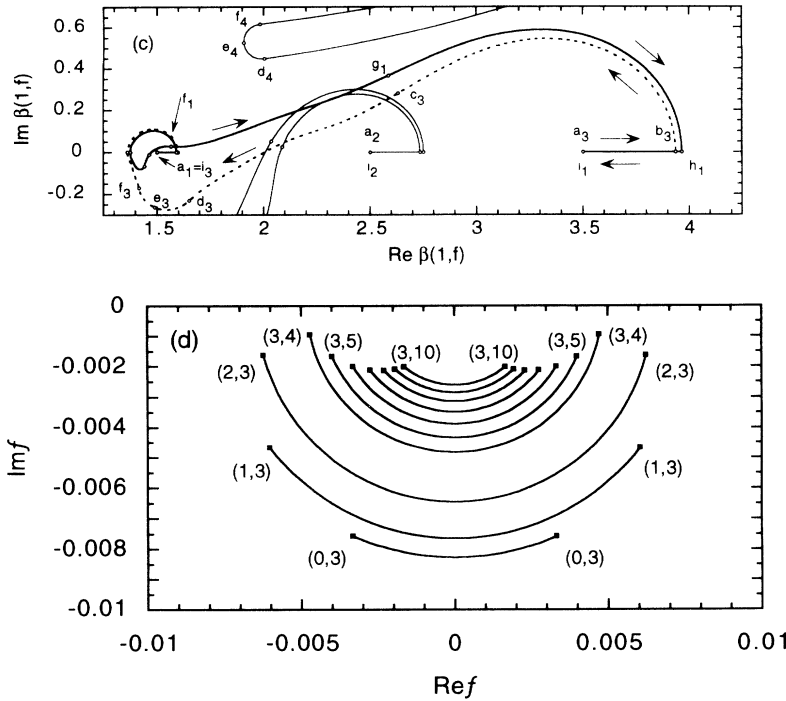


FIG. 2 (Continued).

(0,3) has been drawn. (To have drawn more would have cluttered the figure.) The starting and key intermediate points have been labeled from a to i . We plot in Figs. 2(b) and 2(c) the trajectories of the anharmonic eigenvalues that originate from the four lowest harmonic oscillator eigenvalues when $f = 0$. The images of the starting and intermediate points have been labeled, when feasible, with a_n, b_n, \dots, i_n , where $n = 0, 1, 2, 3, 4$. Note how the trajectories for $n = 0, 2$, and 4 return to their initial values, $0.5, 2.5$, and 4.5 . But the trajectory for $n = 1$ starts at 1.5 and ends at 3.5 , while the trajectory for $n = 3$ starts at 3.5 and ends at 1.5 . Figure 2(c) is a twofold magnification of Fig. 2(b) to show the region from $\beta(1, f) \sim 1.5$ to $\beta(1, f) \sim 3.5$ in greater detail. The eigenvalues connected at this branch point are not adjacent.

Numerically we find that for *any pair* of anharmonic oscillator levels there are exactly four values of the anharmonicity constant f at which these levels cross. Each branch point appears on precisely two triple sheets and on no others. That is, for any triple sheet T_n , only those branch points in Fig. 1 that have n as one of their two labels can be encountered. Those branch points that do not involve n are not branch points on T_n . Figure 2(d) illustrates the branch points and cuts in the third and fourth quadrants of the first sheet of T_3 ; the pattern is typical. It is in the sense of this picture that the Riemann surface put forward by Bender and Wu needs modification.

C. Modification of the Bender-Wu surface

To describe more completely the Riemann surface of $\beta(1, f)$, we recall a few points made by Bender, Wu, and Simon that follow from Symanzik scaling and that the Hamiltonian $H(1, f)$ [Eq. (6)] is self-adjoint for real, positive f .

itive f .

We have already remarked that the origin is a cubic-root global branch point and that the primary unit of the Riemann surface for $\beta(1, f)$ is a triple sheet. Following the notation of Bender and Wu [26], we denote as the first sheet ($0 \leq \arg f < 2\pi$), the second sheet ($2\pi \leq \arg f < 4\pi$), and the third sheet ($4\pi \leq \arg f < 6\pi$) = $(-2\pi \leq \arg f < 0)$, (mod 6π). Note that analytic continuation by exactly 3π [cf. Eqs. (9) and (11)] gives an eigenvalue spectrum that is the negative of the f spectrum:

$$\beta(1, e^{i3\pi} f) = -\beta(1, f). \tag{33}$$

The second point is a consequence of the Schwarz reflection principle (i.e., real power series for real f),

$$\beta(1, |f|e^{i \arg f}) = \beta(1, |f|e^{i(6\pi - \arg f)})^*. \tag{34}$$

The third follows from Eqs. (33) and (34): for $\arg f = 3\pi/2$ and $9\pi/2$ ($-3\pi/2$), the eigenvalues are pure imaginary. This result also follows directly from rescaling the eigenvalue equation. For instance, for $\arg f = 3\pi/2$, Eq. (22) permits using $\arg s = -\pi/2$. With s replaced by $-is$, the eigenvalue equation becomes

$$\left(-s \frac{d^2}{ds^2} + \frac{m^2 - 1}{4s} - \frac{1}{4}s + |f|s^2 \right) \phi(s) = -i \beta(1, |f|e^{i3\pi/2}) \phi(s), \tag{35}$$

which has the form of a real eigenvalue equation save for $-i$ times the eigenvalue parameter.

These properties have direct consequences on the location of the Bender-Wu branch points—that they come in groups of four. In particular, Eqs. (33) and (34) show

that if f_c is a branch point, then so are its reflection across the imaginary axis $|f_c|e^{i(3\pi-\arg f_c)}$ and the two obtained from these by rotation by 3π , $f_c e^{i3\pi}$ and $|f_c|e^{i(6\pi-\arg f_c)}$. The four can be coupled into two pairs, one pair symmetrically placed in the third and fourth quadrants of the first sheet and the other pair symmetrically placed in the first and second quadrants of the third sheet. Hereafter we will add as a superscript $f_c^{(i)}$ ($i=1,2,3,4$) the quadrant in which each branch point lies.

Branch cuts can be drawn between the two members within each pair. It is convenient to draw the cuts on the arcs $|f| = |f_c|$, as has been done in Fig. 2(a) for $f_{03}^{(3)}$ and $f_{03}^{(4)}$ and in Fig. 2(d); this specification of the cuts completes the recipe given in Sec. IIIB for the $\beta(1, f)$ on the triple sheet T_n .

The branch points accumulate at the origin, but with what phase? The answer depends on the subsequence. Consider the quarter of the branch points that lie in the third quadrant of the first sheet, which we denote by $f_{n_1 n_2}^{(3)}$ ($n_1 = 0, 1, 2, \dots$, $n_2 = n_1 + 1, n_1 + 2, \dots$). (The ordering of the labels n_1 and n_2 in $f_{n_1 n_2}^{(i)}$ is unimportant; $f_{n_1 n_2}^{(i)}$ is the same as $f_{n_2 n_1}^{(i)}$.) We examined the limits of two subsequences numerically and found that $\lim_{n_2 \rightarrow \infty} \arg f_{n_1 n_2}^{(3)} = 3\pi/2$, while $\lim_{n_1 \rightarrow \infty} \arg f_{n_1 n_1+1}^{(3)} = \pi$, as can be inferred from Fig. 1(a). The first result was proved rigorously by Simon (see Corollary II.10.4 of Ref. [29]). The second result could have been inferred from Ref. [26] if it had been possible to assign the branch points correctly.

We summarize the topological aspects of our discussion by noting that the whole Riemann surface consists of an infinite number of triple sheets T_n , each labeled by the quantum number of an anharmonic oscillator eigenvalue for the real self-adjoint equation. Any pair of triple sheets, for instance, T_{n_1} and T_{n_2} , associated with the n_1 th and n_2 th eigenvalues, is connected by exactly two branch cuts, one connecting the first sheets of the respective triple sheets and the second connecting the third sheets. One can pass directly from one triple sheet to any other.

D. Trajectories for $\beta(1, |f|e^{i\theta})$ as f traverses a triple circle; picture of a typical crossing

In this subsection we examine the trajectories of $\beta(1, |f|e^{i\theta})$ as θ runs from 0 to 6π . Some aspects have not been anticipated in prior work, and it is possible to give a detailed picture of the crossing of eigenvalues when f passes through a branch point.

1. Large-scale picture

Figures 3(a)–3(e) show the paths traveled in the complex plane by the four lowest $m = 0$ resonances, corresponding to $n = 0, 1, 2, 3$, for five values of $|f|$, all with $\theta \in [0, 6\pi]$. Figures 3(a)–3(e) have $|f| = 0.080, 0.040, 0.020, 0.018$, and 0.010 , respectively.

Notice in Fig. 3(a) that as n increases from 0 to 3, the

trajectories become more circular, which is a combined consequence of Symanzik scaling, Eq. (11), and that as n increases, the quadratic potential in Eq. (6) has a diminishing effect as a perturbation of the quartic oscillator. That is, for large f , or for any f and large enough n , as f moves along a triple circle, $\beta(1, f)$ is approximately $f^{1/3}$ times an unperturbed quartic oscillator eigenvalue

$$\beta(1, f) = f^{1/3}\beta(f^{-2/3}, 1) \sim f^{1/3}\beta(0, 1). \quad (36)$$

Already in Fig. 3(a), however, the $n = 0$ trajectory is far from circular, and the outer three are flattened. As $|f|$ decreases to 0.040 [Fig. 3(b)], all the trajectories contract, the outer three flatten further, and the pinched sections of the $n = 0$ trajectory intersect each other to form a three-lobed figure. By $|f| = 0.020$ [Fig. 3(c)—note the change in scale between Figs. 3(b) and 3(c)], the $n = 0$ middle lobe dwarfs the outer two, and the $n = 1$ trajectory has become severely pinched. There is an abrupt change in the topology between $|f| = 0.020$ and 0.018 [Fig. 3(d)]: The $n = 0$ and $n = 1$ trajectories *seem to have exchanged their “middle” parts*. This is a consequence of the $|f| = 0.020$ and $|f| = 0.018$ triple circles being separated by the $f_{01}^{(i)}$ branch points, which have $|f_{01}^{(i)}| = 0.018\,838\,404\,078\,069\,6$. Figure 3(e) at $|f| = 0.010$ shows the increasing intricacy as $|f|$ has been decreased past the second quartet of branch points $f_{02}^{(i)}$, which fall on $|f| = 0.011\,654\,854\,413\,201\,8$.

2. Details of a recombinant crossing

The T_0 and T_1 triple sheets have a common branch point at $|f_{01}^{(3)}| = 0.018\,838\,404\,078\,069\,6$, $\arg f_{01}^{(3)} = 3.804\,652\,181\,161\,366\,1$, as indicated in Table I. The behavior of the $n = 0$ and $n = 1$ trajectories of $\beta(1, f)$ for fixed $|f|$, as $|f|$ passes through this value, are shown in detail in Fig. 4. The case that $|f| = |f_{01}^{(3)}|$ is shown in Fig. 4(b). When $|f|$ is a little larger [Fig. 4(a)], the $n = 0$ trajectory approaches the image of the branch point $f_{01}^{(3)}$ and then turns down sharply, while the $n = 1$ trajectory turns up. When $|f| = |f_{01}^{(3)}|$, the sharp turns become right angles, at the vertices of which the two trajectories touch. As $|f|$ decreases from $f_{01}^{(3)}$, the trajectories “break” and “recombine” as they exchange the outgoing legs of their right angles [Fig. 4(b) to Fig. 4(c)]. The gross appearance is that the “identities” of the trajectories after the region of the branch point have been exchanged. One can see immediately how if $\beta(1, f)$ started out on the $n = 0$ sheet, and if f circled the branch point $f_{01}^{(3)}$ and returned to $\theta = 0$, then $\beta(1, f)$ would end up on the $n = 1$ sheet, as illustrated in Fig. 2 for the $f_{13}^{(3)}$ case.

On nomenclature, the trajectories do not literally *cross* at the branch point. The $\beta(1, f)$ *coincide* at the branch point, and the trajectories *exchange segments* or *detach and recombine*.

The 90° character of the trajectory at the branch point is a consequence of the square-root nature of the branch

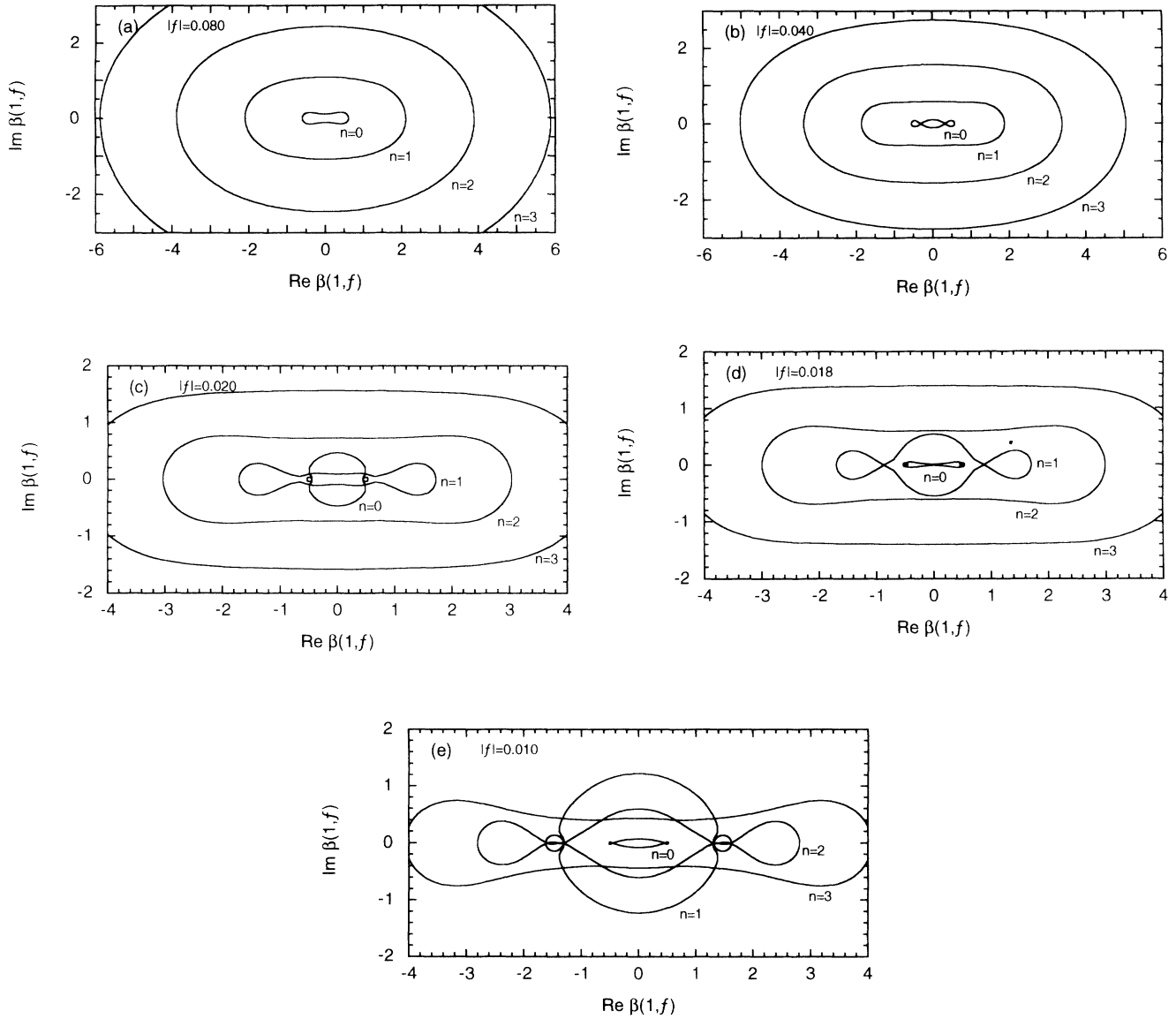


FIG. 3. Trajectories of $\beta(1, f)$ at constant $|f|$, for the branches $n = 0$ through $n = 3$: (a) $|f| = 0.080$; (b) $|f| = 0.040$; (c) $|f| = 0.020$; (d) $|f| = 0.018$; (e) $|f| = 0.010$. Note that the scale for (c)–(e) is magnified versus (a) and (b).

point. If $|f| = |f_{01}^{(3)}|e^{i\theta}$, then by Eq. (27)

$$\beta_{\pm}(1, |f_{01}^{(3)}|e^{i\theta}) \sim \beta(1, f_{01}^{(3)}) \pm a_{1/2} f_{01}^{(3)1/2} \left[e^{i(\theta - \theta_{01}^{(3)})} - 1 \right]^{1/2} \quad (37)$$

$$\sim \beta(1, f_{01}^{(3)}) \pm a_{1/2} f_{01}^{(3)1/2} e^{i\pi/4} (\theta - \theta_{01}^{(3)})^{1/2}. \quad (38)$$

As $(\theta - \theta_{01}^{(3)})$ increases through 0, its square root changes from pure imaginary to real, and the trajectory makes a 90° turn.

3. Anti-Herglotz at large scale, Herglotz at small scale

Consider now Fig. 5(a), on which is plotted $|f| = 0.0001$. According to Table I, many $|f_{0n}^{(3)}|$ and $|f_{1n}^{(3)}|$

branch points are already outside the three-sheeted circle traced by f . For this value of $|f|$, the JWKB method of Bender and Wu is globally quite accurate, and from a distance the trajectories appear uninteresting. But a closer look reveals that the $n = 1$ trajectory seems to dip immediately into the negative half plane. There is a “cut Herglotz” property proved by Simon for the function $\beta(1, f)$ on the f plane cut from 0 to $-\infty$:

$$\frac{\text{Im} \beta(1, f)}{\text{Im} f} > 0. \quad (39)$$

That is to say, the trajectory for $\beta(1, f)$ should start upwards with $\text{Im} f$, and it appears to start downwards in Fig. 5(a). The same is true of every other trajectory in Fig. 3 of Ref. [26]. The explanation can be uncovered by blowing up the scale of the plot at the beginning of the trajectories, as shown in Figs. 5(b) and 5(c). The

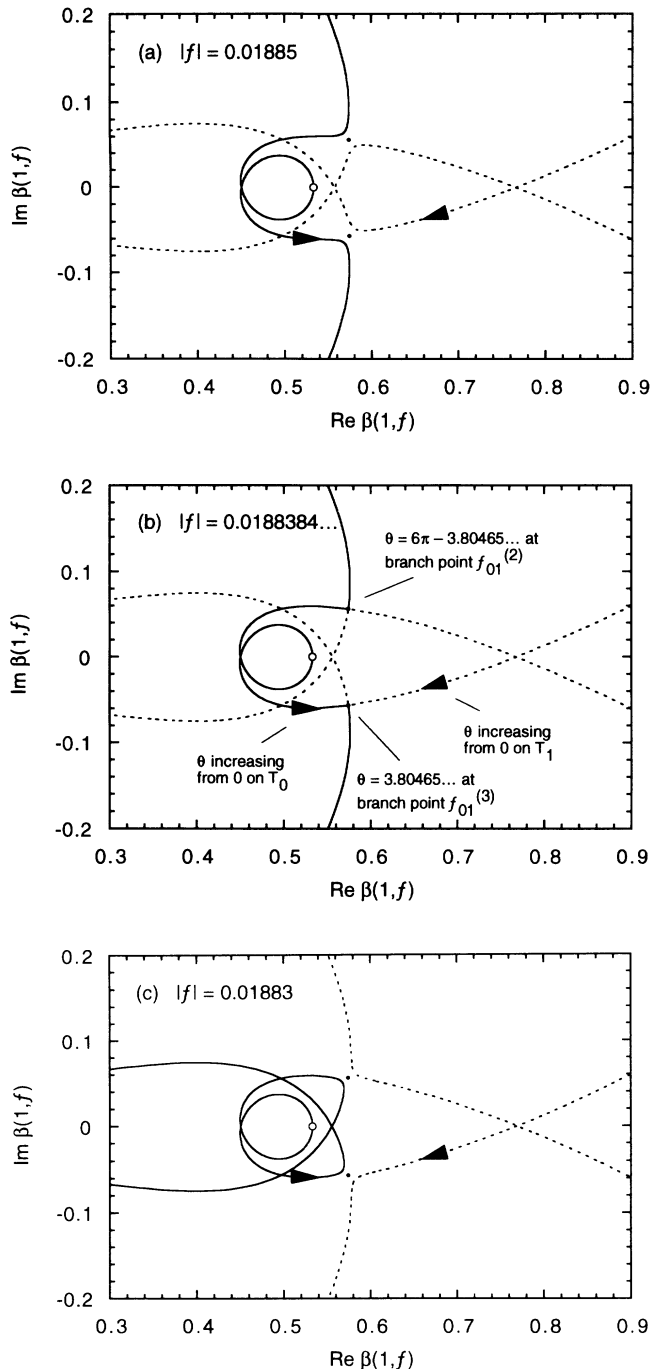


FIG. 4. Details of trajectory recombination at a branch point. Solid line, the $n = 0$ trajectory; dashed line, the $n = 1$ trajectory; solid circles, the branch points $f_{01}^{(3)}$ (lower) and $f_{01}^{(2)}$ (upper); open circle, the beginning of the $n = 0$ trajectory at $\theta = 0$. The arrowheads indicate the direction of increasing θ just before the vicinity of the branch point $f_{01}^{(3)}$ at $\theta = 3.8046521811613661$. (a) Just outside the (01) branch cuts, $|f| = 0.01885$. (b) Right at the (01) branch cuts, $|f| = 0.0188384040780696$. Note how the two trajectories enter the images of the branch points collinearly and leave collinearly, but perpendicularly to the incoming direction. (c) Just inside the (01) branch cuts, $|f| = 0.01883$. Notice how the outgoing trajectories have “detached” and “recombined” with the opposite incoming trajectories. What happens at $f_{01}^{(3)}$ on the first sheet is mirrored at $f_{01}^{(2)}$ on the third sheet.

semicircular arcs from $\theta = 0$ to π are accurately given by first-order perturbation theory:

$$\beta(1, f) \sim \beta(1, 0) + (6n^2 + 6n + 2 + m^2 + 3|m| + 6n|m|)f. \quad (40)$$

Thus, on the one hand, the apparent “wrong direction” is strictly an artifact of low resolution, while on the other, the sharp twists visible at high resolution are somewhat unexpected and are driven by nearby Bender-Wu branch points.

IV. SEPARATION CONSTANTS OF LoSURDO-STARK RESONANCES

In the preceding section we located and labeled the Bender-Wu branch points, and we showed the behavior of the eigenvalues along simple f contours. We now use this information to understand the LoSurdo-Stark resonances at large F for a typical set of resonances, those with principal quantum number $n = 4$. There are experimental data for $n = 4$ up to moderately high fields (see Ref. [20]), and the states of this manifold illustrate all the different behaviors we have found.

The LoSurdo-Stark resonances of atomic hydrogen solve the system of Eqs. (4), (5), and (7) with $Z = 1$ and $k = -2E$ scaled out, i.e.,

$$\left(-s \frac{d^2}{ds^2} + \frac{m^2 - 1}{4s} + \frac{1}{4}s + fs^2\right) \phi_1(s) = \beta_1 \phi_1(s), \quad (41)$$

$$\left(-s \frac{d^2}{ds^2} + \frac{m^2 - 1}{4s} + \frac{1}{4}s + fe^{-i\pi}s^2\right) \phi_2(s) = \beta_2 \phi_2(s), \quad (42)$$

$$\beta_1(1, f) + \beta_2(1, e^{-i\pi}f) = (4f/F)^{1/3}. \quad (43)$$

To be consistent with the definition of resonance, that $\text{Im}\beta_2 < 0$ for positive f , the $-F$ in Eq. (5) must be understood as $Fe^{-i\pi}$, as indicated by the $fe^{-i\pi}$ in Eq. (42).

In contrast with the preceding section, where the f contours were chosen to illustrate various points, here the contour for f is completely specified by the system of Eqs. (41)–(43). That is, $f(F)$ is a function obtained by solving the system of equations, starting with a given set of parabolic quantum numbers (n_1, n_2, m) at $F = 0$.

With the numerical method of Ref. [22] we have tracked the ten states with principal quantum number $n = 4$ as the electric field increases from zero to infinity. Our numerical calculations show, independent of the state, that the scaled field f starts at the origin and traces a closed loop in the third “global” Riemann sheet, i.e., $-2\pi \leq \arg f \leq 0 \pmod{6\pi}$. The only branch points f or $fe^{-i\pi}$ can encounter are those with $-2\pi < \arg f < -\pi$. The trajectories we have calculated all fall into three categories.

The first occurs when the initial state (n_1, n_2, m) has

$n_1 = n_2$ and is illustrated by $(1, 1, 1)$ in Fig. 6. The coupling constant f traces an oval path in the lower half plane of the third Riemann sheet, where there are no branch points, while the oval for $fe^{-i\pi}$ in the upper half plane loops all pairs of branch points, but no branch cut is crossed. Only $m = 1$ branch points with labels $(1, n)$ can be seen by $\beta_1(1, f)$ or $\beta_2(1, fe^{-i\pi})$, and in Fig. 6 the first few pairs are shown. At $F = \infty$, β_1 returns to its initial value, while β_2 returns to the negative of its initial value. (The initial values of β_1 and β_2 are the same for

this case.)

The second category occurs when $n_1 > n_2$ and is illustrated by $(3, 0, 0)$ in Fig. 7. The scaled field f starts out tracing a smooth oval in the lower half plane of the third Riemann sheet where there are no branch points, but before returning to the origin, it crosses the negative real axis and encircles exactly one branch point, the one denoted $f_{n_2 n_1}^{(2)} = f_{03}^{(2)}$ in Sec. III, and then returns to the origin where β_1 now has the initial value of β_2 . At the same time, $fe^{-i\pi}$ crosses no branch cuts and β_2 ends up

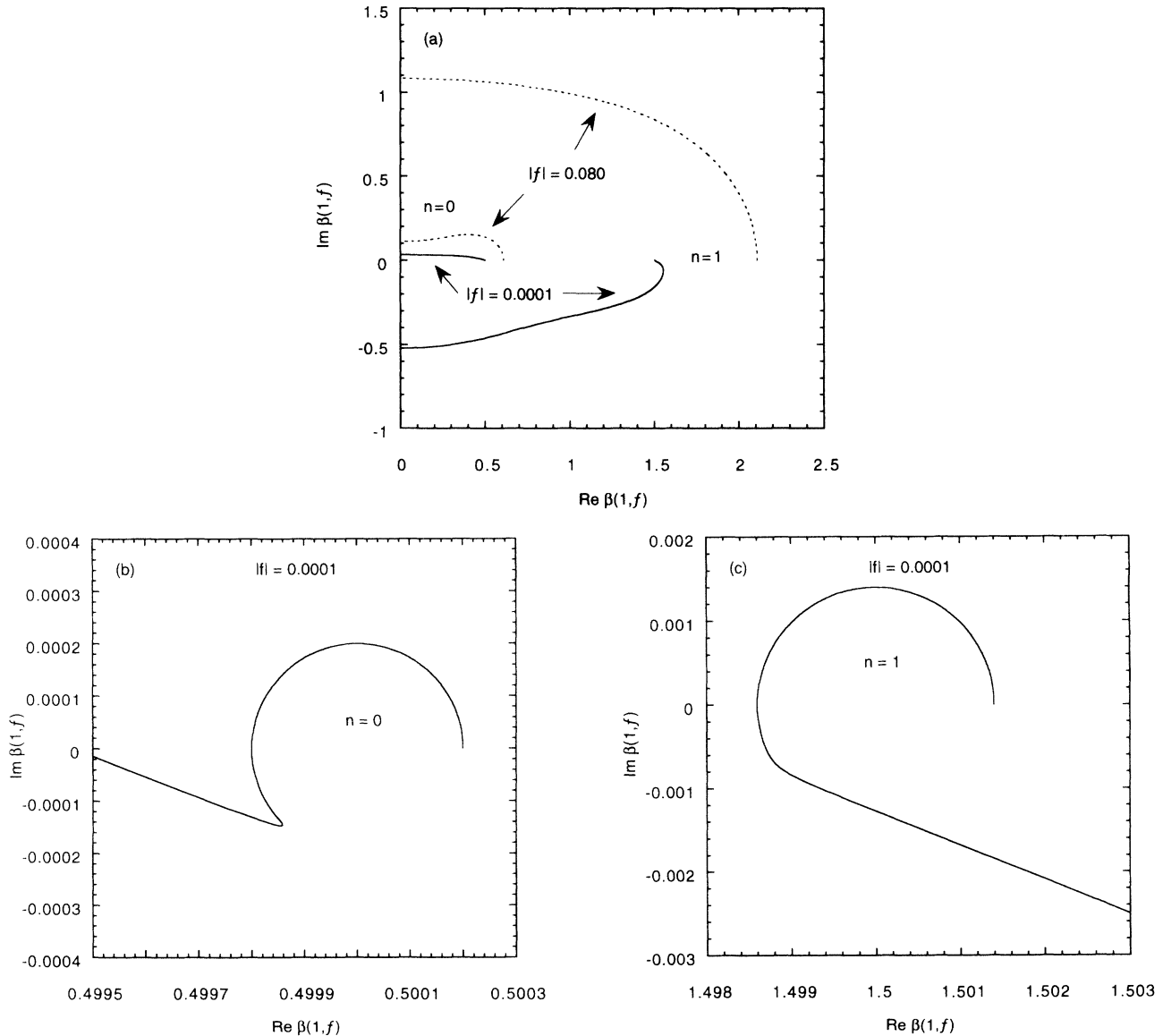


FIG. 5. Possibly misleading anti-Herglotz appearance of constant- $|f|$ trajectories when $|f|$ is small. (a) $n = 0$ and $n = 1$ constant- $|f|$ trajectories of $\beta(1, |f|e^{i\theta})$ for $|f| = 0.0800$ (dashed lines) and $|f| = 0.0001$ (solid lines), with $\theta \in [0, 3\pi/2]$. The two plots for $|f| = 0.0800$ constitute one-quarter $[3\pi/2 \text{ vs } 6\pi]$ of the same plots given in Fig. 3(a) and are reproduced here for reference. At $\theta = 3\pi/2$, $\beta(1, |f|e^{i\theta})$ always falls on the imaginary axis. The Herglotz property requires that $\text{Im } \beta(1, f) > 0$ when $0 < \arg f < \pi$. Unlike the other three, the $n = 1$ trajectory for $|f| = 0.0001$ appears to start out with negative imaginary part, even though $\text{Im } f$ starts out positive. (b) Greatly magnified blowup of the $\theta = 0$ end of the $n = 0$ trajectory. (c) Greatly magnified blowup of the $\theta = 0$ end of the $n = 1$ trajectory. Both show structure not visible at the scale of (a). In this microscopic view, it is clear that the Herglotz condition is satisfied and that the $n = 1$ trajectory does not begin its plunge into the negative half plane until θ has exceeded π .

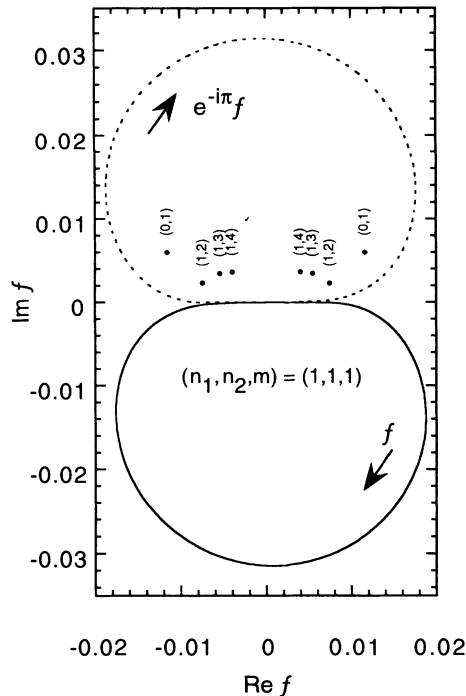


FIG. 6. Trajectories as F increases from 0 to ∞ for $f(F)$ (solid line) and $e^{-i\pi}f(F)$ (dashed line) on the $\beta_1(1, f)$ and $\beta_2(1, fe^{-i\pi})$ Riemann surface for the resonance $(n_1, n_2, m) = (1, 1, 1)$, for which $n_1 = n_2$. Only $(n, 1)$ branch points appear on the third sheet of the relevant T_1 triple sheet. No branch cuts are crossed, but the $e^{-i\pi}f(F)$ trajectory loops all the branch cuts. $\beta_1(1, f)$ returns to its initial value ($= 2$), while $\beta_2(1, fe^{-i\pi})$ returns to the negative of its initial value ($= -2$).

at $F = \infty$ with the negative of its initial value. Figure 7(a) shows the entire trajectories for f and $fe^{-i\pi}$. On this scale the branch points cannot be seen. Figure 7(b) is a blowup of the region where $\beta_1(1, f)$ slices through the $(0, 3)$ branch cut. While f is on the $n = 3$ triple sheet T_3 , $\beta_1(1, f)$ “sees” only $(n, 3)$ branch points, which are the only ones shown in Fig. 7(b). The trajectory appears to cross not only the $(0, 3)$ branch cut, but also $(1, 3)$, $(2, 3)$, $(3, 4)$, and $(3, 5)$ as well, but this is an artifact of the diagram. As soon as f passes through the $(0, 3)$ cut, f is on T_0 , and none of the other $(n, 3)$ branch points are visible: instead f now sees only $(0, n)$ branch points, as plotted in Fig. 7(c).

The third category occurs when $n_1 < n_2$ and is illustrated by $(0, 3, 0)$ in Fig. 8. The scaled field f stays completely in the lower half plane of the third Riemann sheet where there are no branch points, and when $F = \infty$, β_1 returns to its initial value. Meanwhile, $fe^{-i\pi}$ stays completely in the upper half plane. But unlike the first two cases, the trajectory of $fe^{-i\pi}$ passes through exactly one branch cut, the one joining $f_{03}^{(2)}$ and $f_{03}^{(1)}$, and then returns to the origin where β_2 now has the negative of the initial value of β_1 . The $(n, 3)$ branch points are shown in Fig. 8(a). They are visible to $\beta_2(1, fe^{-i\pi})$ at the beginning of the trajectory. When $fe^{-i\pi}$ passes through the $(0, 3)$ branch cut, only the $(0, n)$ branch points are visi-

ble, as is shown in Fig. 8(b). Note in Fig. 8(b) that the trajectory of $fe^{-i\pi}$ passes to the right of all the $(0, n)$ branch cuts ($n \geq 4$), while in Fig. 7(c) the trajectory of f passes to the left of the same branch cuts. This is why $\beta_2(1, fe^{-i\pi})$ ends up at the negative of $\beta_1(1, 0)$ in the $(0, 3, 0)$ case, while $\beta_1(1, f)$ ends up equaling (the positive) $\beta_2(1, 0)$ in the $(3, 0, 0)$ case.

We do not have a general proof, but this behavior has been confirmed in all the cases we have tested: If $n_1 \neq n_2$, the coupling constant of the equation corresponding to the largest separation constant at zero field crosses the $n_1 \leftrightarrow n_2$ branch cut, and as the electric field F tends to infinity, $\beta_1 \rightarrow \min(\beta_1^{(0)}, \beta_2^{(0)})$, $\beta_2 \rightarrow -\min(\beta_1^{(0)}, \beta_2^{(0)})$.

V. ASYMPTOTIC BEHAVIOR OF LoSURDO-STARK RESONANCES AT LARGE FIELD

The numerical study of the preceding section showed that as $F \rightarrow \infty$, the scaled field $f \rightarrow 0$ with asymptotic phase $-\pi \pmod{6\pi}$, and the separation constants approach \pm a common unperturbed eigenvalue. In this section we use this information in deriving an asymptotic formula for $E(F)$.

A. Starting formulas

Let

$$n_\infty = \min(n_1, n_2). \quad (44)$$

An empirical result of Sec. IV is that as $F \rightarrow \infty$, $\beta_1 \rightarrow n_\infty + (m + 1)/2$, and, $\beta_2 \rightarrow -[n_\infty + (m + 1)/2]$. Near $F = \infty$ both separation constants have values on the same triple sheet corresponding to n_∞ , β_1 at $\arg f = -\pi = 5\pi \pmod{6\pi}$, and β_2 at $\arg(fe^{-i\pi}) = 4\pi$. It is convenient to use the notation $\beta(1, f)$ for β_1 , because for β_2 on the same triple sheet it follows with the aid of Eq. (33) that $\beta_2 = \beta(1, fe^{-i\pi}) = -\beta(1, fe^{i2\pi})$. The implicit Eq. (43) for $f(F)$ then becomes

$$\beta(1, f) - \beta(1, fe^{i2\pi}) = \left(\frac{4f}{F}\right)^{1/3}. \quad (45)$$

The left-hand side of Eq. (45) is the discontinuity of $\beta(1, f)$ between two successive sheets of the triple sheet belonging to n_∞ . The region of interest is $\arg f \approx -\pi$, so that the discontinuity is at the negative real axis between the third and first sheets. Reference [15] gives an asymptotic expansion for the discontinuity (45), valid for $-3\pi/2 < \arg f < -\pi/2$ and $|f|$ sufficiently small:

$$\begin{aligned} & \beta(1, f) - \beta(1, fe^{i2\pi}) \\ & \sim -i \frac{(-f)^{-2\beta_\infty}}{n_\infty!(n_\infty + m)!} \exp\left(\frac{1}{6f}\right) \sum_{N=0}^{\infty} b_\infty^{(N)} (-f)^N, \end{aligned} \quad (46)$$

where

$$\beta_\infty = n_\infty + (m + 1)/2 \tag{47}$$

and the $b_\infty^{(N)}$ are known functions of β_∞ and m [6,15]. For example,

$$b_\infty^{(0)} = 1, \tag{48}$$

$$b_\infty^{(1)} = -34\beta_\infty^2 - 12\beta_\infty - \frac{5}{3} + \frac{3}{2}(m^2 - 1), \tag{49}$$

$$b_\infty^{(2)} = 578\beta_\infty^4 - 92\beta_\infty^3 - \frac{442}{3}\beta_\infty^2 - 90\beta_\infty - \frac{155}{18} - 51(m^2 - 1)\beta_\infty^2 + 25(m^2 - 1)\beta_\infty + \frac{13}{2}(m^2 - 1) + \frac{9}{8}(m^2 - 1)^2. \tag{50}$$

All the asymptotic expansions derived below follow from Eqs. (45) and (46).

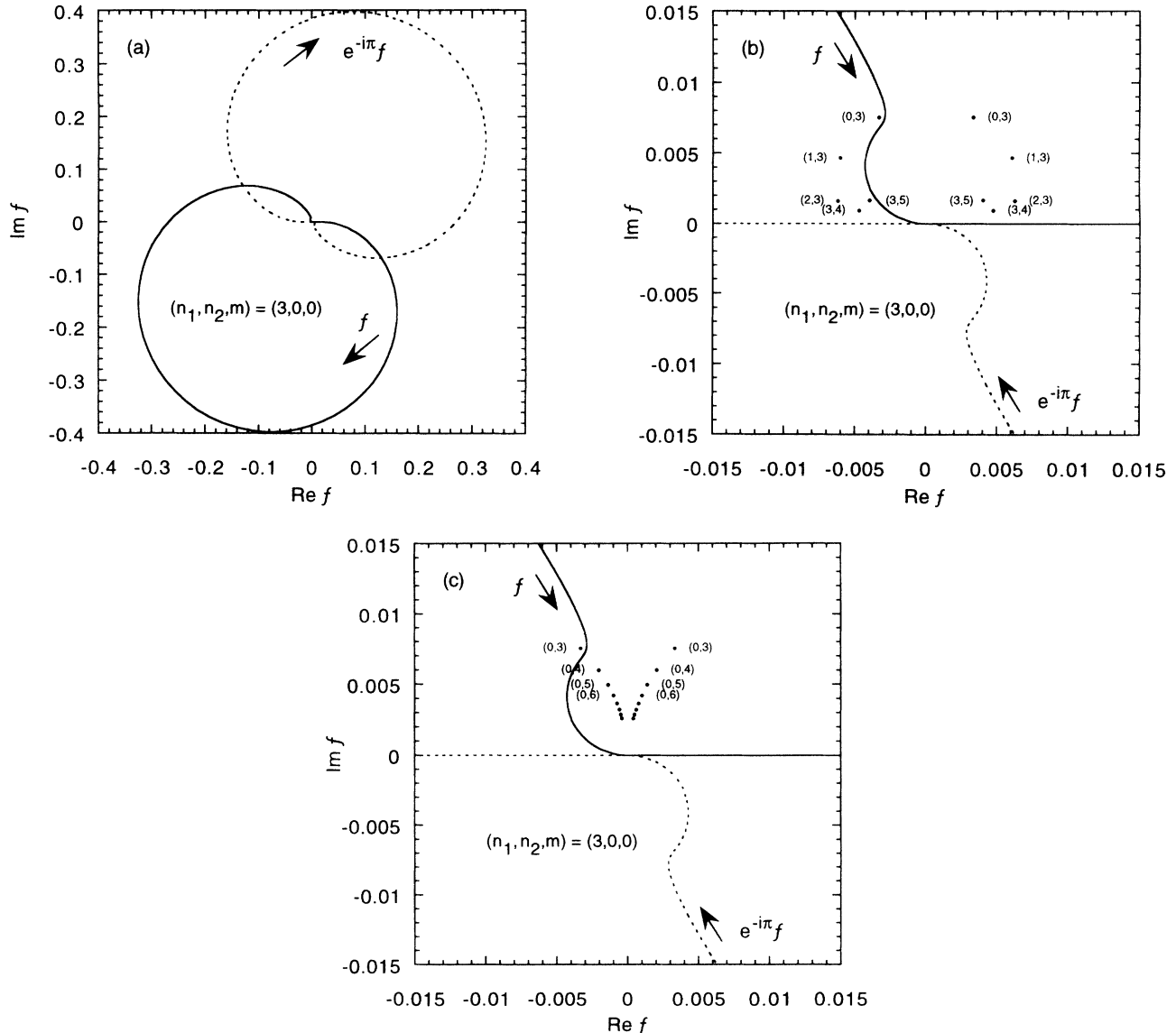


FIG. 7. Trajectories as F increases from 0 to ∞ for $f(F)$ (solid line) and $e^{-i\pi}f(F)$ (dashed line) on the $\beta_1(1, f)$ and $\beta_2(1, fe^{-i\pi})$ Riemann surface for the resonance $(n_1, n_2, m) = (3, 0, 0)$, for which $n_1 > n_2$. (a) Large-scale view of the trajectories. Notice that f loops into the lower half plane (third sheet of T_3), but swings into the upper half plane before returning to the origin. (b) Blowup of the region near the origin to show the Bender-Wu branch points. Initially the only relevant branch points to f are the $(n, 3)$ on T_3 , which are shown. The trajectory for f crosses the $f_{03}^{(2)} - f_{03}^{(1)}$ branch cut onto the triple sheet T_0 . (c) Blowup of the region near the origin with the $(0, n)$ branch points on T_0 shown. These are the ones visible to f after passing through the $f_{03}^{(2)} - f_{03}^{(1)}$ cut. None of the other $(0, n)$ branch cuts are crossed. These are also the branch points visible to $fe^{-i\pi}$, which does not cross any branch cut, but encircles all of them. $\beta_1(1, f)$ returns at $F = \infty$ to the initial value of $\beta_2, 1/2$, while $\beta_2(1, fe^{-i\pi})$ returns to the negative of its initial value, $-1/2$.

B. Trajectory equation: $\arg f$ as a function of $|f|$

To obtain asymptotic equations for the modulus and argument of f , we first substitute Eq. (46) for the discontinuity into Eq. (45) and indicate separately the modulus and argument of f to obtain

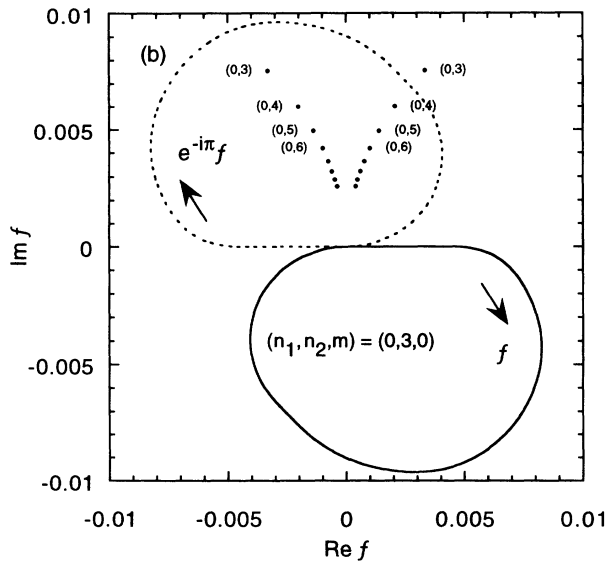
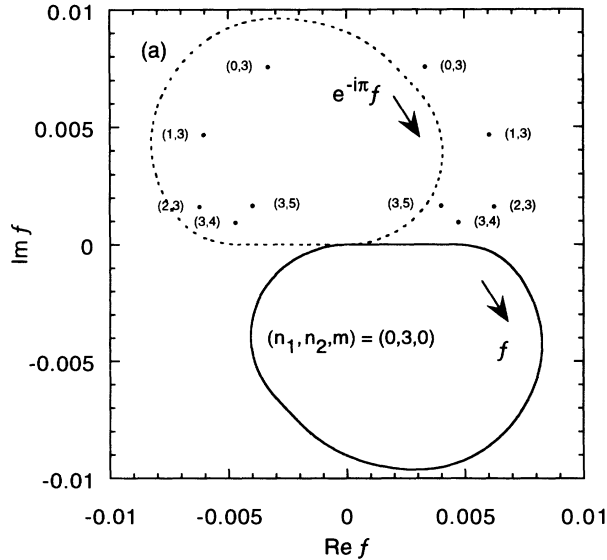


FIG. 8. Trajectories as F increases from 0 to ∞ for $f(F)$ (solid line) and $f(F)e^{-i\pi}$ (dashed line) on the $\beta_1(1, f)$ and $\beta_2(1, fe^{-i\pi})$ Riemann surface for the resonance $(n_1, n_2, m) = (0, 3, 0)$, for which $n_1 < n_2$. The trajectory for f lies entirely in the lower half plane (third sheet of T_0), where there are no branch points. $\beta_1(1, f)$ returns to its initial value, $1/2$, at $F = \infty$. The trajectory for $fe^{-i\pi}$ starts off on the third sheet of T_3 and passes through the $f_{03}^{(2)} - f_{03}^{(1)}$ cut onto T_0 . (a) The view from T_3 of the trajectories and branch points. (b) The view from T_0 : The trajectory for $fe^{-i\pi}$ passes to the right of all subsequent branch cuts and $\beta_2(1, fe^{-i\pi})$ ends up with the negative of the initial value of β_1 , $-1/2$.

$$-i \frac{(|f|e^{i(\arg f + \pi)})^{-2\beta_\infty}}{n_\infty! (n_\infty + m)!} \exp\left(\frac{1}{6|f|e^{i\arg f}}\right) \times \sum_{N=0}^{\infty} b_\infty^{(N)} (|f|e^{i(\arg f + \pi)})^N \sim \left(\frac{4|f|e^{i\arg f}}{F}\right)^{1/3}. \quad (51)$$

Next we set equal the arguments of both sides of Eq. (51) (the magnitudes will be treated later):

$$-\frac{\pi}{2} - 2\beta_\infty(\arg f + \pi) - \frac{\sin(\arg f)}{6|f|} + \arg\left(\sum_{N=0}^{\infty} b_\infty^{(N)} (|f|e^{i(\arg f + \pi)})^N\right) \sim \frac{1}{3} \arg f + 2k\pi, \quad (52)$$

where $k = 0, \pm 1, \pm 2, \dots$ [the integer k here is not to be confused with the “force constant k ” in Eqs. (6) and (23)].

Since Eq. (52) does not depend explicitly on F , it can be solved for $\arg f$ as a function of $|f|$. That is, it is an equation for the (large- F) end of the trajectory in the f plane for all states ending up with a particular n_∞ (and m). Notice that only one of the two quantum numbers (n_1, n_2) appears explicitly via n_∞, β_∞ , and the $b_\infty^{(N)}$. The second comes in via k . [See Eq. (60) below.]

We look for a series solution

$$\arg f \sim -\pi + a^{(1)}|f| + a^{(2)}|f|^2 + a^{(3)}|f|^3 + \dots \quad (53)$$

Because of the way that k and β_∞ enter the $a^{(i)}$, the formulas are a little simpler if we define

$$q = (12k + 1)\pi, \quad (54)$$

$$s_\infty = 2(6\beta_\infty + 1). \quad (55)$$

One finds that

$$a^{(1)} = q, \quad (56)$$

$$a^{(2)} = qs_\infty, \quad (57)$$

$$a^{(3)} = q\left(\frac{1}{6}q^2 + s_\infty^2 - 6b_\infty^{(1)}\right), \quad (58)$$

$$a^{(4)} = q\left(\frac{2}{3}q^2s_\infty + s_\infty^3 - 12b_\infty^{(1)}s_\infty + 6b_\infty^{(1)2} - 12b_\infty^{(2)}\right). \quad (59)$$

For each integer k there is a different solution for $\arg f$. All the solutions for $\arg f$ approach $-\pi$, but the slope of each is different, corresponding to $q = (12k + 1)\pi$. Note that the trajectories for $f = |f|e^{i\arg f} \sim -|f| - iq|f|^2 + \dots$ all end at -0 with zero slope, but the curves separate as f moves away from the origin. By examining numerical solutions for all the resonances stemming from states with principal quantum number $n \leq 4$, we have

found that in each case k is given by

$$k = n_2 - n_1. \quad (60)$$

C. Expansions for $\arg f$ and $|f|$ as functions of F

We return now to Eq. (51) and equate the magnitudes of both sides:

$$\frac{|f|^{-2\beta_\infty}}{n_\infty!(n_\infty + m)!} \exp\left(\frac{\cos(\arg f)}{6|f|}\right) \times \left| \sum_{N=0}^{\infty} b_\infty^{(N)} (|f|e^{i(\arg f + \pi)})^N \right| \sim \left(\frac{4|f|}{F}\right)^{1/3}. \quad (61)$$

Equation (61) can easily be solved for F in terms of $|f|$ and $\arg f$:

$$\ln \frac{F}{4[n_\infty!(n_\infty + m)!]^3} \sim (6\beta_\infty + 1) \ln |f| - \frac{\cos(\arg f)}{2|f|} - 3 \ln \left| \sum_{N=0}^{\infty} b_\infty^{(N)} (|f|e^{i(\arg f + \pi)})^N \right|. \quad (62)$$

Further, $\arg f$ can be eliminated via Eq. (53) to give an equation for $F(|f|)$ that has the form

$$\ln \frac{F}{4[n_\infty!(n_\infty + m)!]^3} \sim (6\beta_\infty + 1) \ln(|f|) + \frac{1}{2|f|} + \sum_{N=1}^{\infty} d^{(N)} |f|^N. \quad (63)$$

The first couple of $d^{(N)}$ are

$$d^{(1)} = -\frac{1}{4}q^2 - 3b_\infty^{(1)}, \quad (64)$$

$$d^{(2)} = -\frac{1}{2}q^2 s_\infty + \frac{3}{2}b_\infty^{(1)2} - 3b_\infty^{(2)}. \quad (65)$$

What is really needed, however, is not F as a function of $|f|$, but $|f|$ as a function of F , that is, the reversion of Eq. (63). The result is more complicated, because there are terms in $\ln \ln F$ as well as $\ln F$. Some simplification comes from the groupings

$$v = \frac{1}{2 \ln \frac{F}{4[n_\infty!(n_\infty + m)!]^3}} \quad (66)$$

$$\sim \frac{1}{2 \ln F}, \quad (67)$$

$$w = -s_\infty \ln v \quad (68)$$

$$= s_\infty \ln \left(2 \ln \frac{F}{4[n_\infty!(n_\infty + m)!]^3} \right) \quad (69)$$

$$\sim 2(6\beta_\infty + 1) \ln(2 \ln F), \quad (70)$$

and from rewriting Eq. (63) in the form

$$|f| \sim v - vw|f| + 2v|f| \sum_{N=1}^{\infty} d^{(N)} |f|^N + s_\infty v |f| \ln \left[1 + \left(\frac{|f|}{v} - 1 \right) \right]. \quad (71)$$

One finds for $|f|$ the series

$$|f| \sim v - v^2 w + v^3 \left[-\left(\frac{1}{2}q^2 + 6b_\infty^{(1)}\right) - s_\infty w + w^2 \right] + \dots \quad (72)$$

$$\sim v - v^2 w + \sum_{N=2}^{\infty} v^{N+1} \sum_{p=0}^N f_p^{(N)} w^p. \quad (73)$$

The series for $1/|f|$ is more directly related to that for $|E|$ [cf. Eq. (81) below]:

$$\frac{1}{|f|} \sim \frac{1}{v} + w + v \left[\left(\frac{1}{2}q^2 + 6b_\infty^{(1)}\right) + s_\infty w \right] + \dots \quad (74)$$

$$\sim \frac{1}{v} + w + \sum_{N=1}^{\infty} v^N \sum_{p=0}^N g_p^{(N)} w^p. \quad (75)$$

Although it is not obvious alone from the expansion (73) for $|f|$ that the expansion (75) for $1/|f|$ has no terms of the form $v^N w^{N+1}$ except for the first two (all others have v to at least as high a power as w), it can be readily seen with the aid of $1/(v|f|)$ times Eq. (71).

The series for $\arg f$ in terms of v and w follows from the composition of Eqs. (53) and (73):

$$\arg f \sim -\pi + qv + qv^2(s_\infty - w) + \dots \quad (76)$$

$$\sim -\pi + q \sum_{N=0}^{\infty} v^{N+1} \sum_{p=0}^N \theta_p^{(N)} w^p. \quad (77)$$

The coefficients $f_p^{(N)}$, $g_p^{(N)}$, and $\theta_p^{(N)}$, for $N \leq 3$, are tabulated in Table III.

D. Large- F expansions for $E(F)$

The corresponding expansions for E follow immediately, since

$$\arg E = -\pi - \frac{2}{3} \arg f \quad (78)$$

$$\sim -\pi/3 - \frac{2}{3}qv - \frac{2}{3}qv^2(s_\infty - w) - \frac{2}{3}qv^3 \left[\left(-\frac{1}{3}q^2 - s_\infty^2 - 12b_\infty^{(1)}\right) - 3s_\infty w + w^2 \right] + \dots \quad (79)$$

$$\sim -\pi/3 - \frac{2}{3}qv \sum_{N=0}^{\infty} v^N \sum_{p=0}^N \theta_p^{(N)} w^p, \quad (80)$$

$$|E| = \frac{1}{2} \left| \frac{F}{4f} \right|^{2/3} \quad (81)$$

$$\sim \frac{1}{2} \left| \frac{F}{4v} \right|^{2/3} \left\{ 1 + \frac{2}{3}vw + v^2 \left[\left(\frac{1}{3}q^2 + 4b_\infty^{(1)}\right) + \frac{2}{3}s_\infty w - \frac{1}{9}w^2 \right] + \dots \right\} \quad (82)$$

$$\sim \frac{1}{2} \left| \frac{F}{4v} \right|^{2/3} \sum_{N=0}^{\infty} v^N \sum_{p=0}^N e_p^{(N)} w^p. \quad (83)$$

TABLE III. The coefficients for the large- F asymptotic expansions of $|f|$, $1/|f|$, $\arg E$, and $|E|$ given in Eqs. (73), (75), (80), and (83), respectively.

| Formulas | | | | | |
|---|-----|--|--|--|--|
| $ f \sim \sum_{N=0}^{\infty} v^{N+1} \sum_{p=0}^N f_p^{(N)} w^p$ | | $1/ f \sim 1/v + w + \sum_{N=1}^{\infty} v^N \sum_{p=0}^N g_p^{(N)} w^p$ | | | |
| $\arg E \sim -\frac{1}{3}\pi - \frac{2}{3}qv \sum_{N=0}^{\infty} v^N \sum_{p=0}^N \theta_p^{(N)} w^p$ | | $ E \sim \frac{1}{2} \left \frac{1}{4} F/v \right ^{2/3} \sum_{N=0}^{\infty} v^N \sum_{p=0}^N e_p^{(N)} w^p$ | | | |
| $v = 1/\left[2 \log \left(\frac{1}{4[n_{\infty}!(n_{\infty}+m)!]^3 F} \right)\right]$ | | $w = s_{\infty} \log \left[2 \log \left(\frac{1}{4[n_{\infty}!(n_{\infty}+m)!]^3 F} \right) \right]$ | | | |
| $q = [12(n_2 - n_1) + 1]\pi$ | | $s_{\infty} = 2(6\beta_{\infty} + 1)$ | | | |
| Coefficients | | | | | |
| N | p | $f_p^{(N)}$ | $g_p^{(N)}$ | $\theta_p^{(N)}$ | $e_p^{(N)}$ |
| 0 | 0 | 1 | 0 | 1 | 1 |
| 1 | 1 | -1 | s_{∞} | -1 | $\frac{2}{3}$ |
| | 0 | 0 | $\frac{1}{2}q^2 + 6b_{\infty}^{(1)}$ | s_{∞} | 0 |
| 2 | 2 | 1 | $-\frac{1}{2}s_{\infty}$ | 1 | $-\frac{1}{9}$ |
| | 1 | $-s_{\infty}$ | $-\frac{1}{2}q^2 + s_{\infty}^2 - 6b_{\infty}^{(1)}$ | $-3s_{\infty}$ | $\frac{2}{3}s_{\infty}$ |
| | 0 | $-\frac{1}{2}q^2 - 6b_{\infty}^{(1)}$ | $\frac{3}{2}q^2 s_{\infty} + 6s_{\infty} b_{\infty}^{(1)}$ $-3b_{\infty}^{(1)2} + 6b_{\infty}^{(2)}$ | $-\frac{1}{3}q^2 + s_{\infty}^2 - 12b_{\infty}^{(1)}$ | $\frac{1}{3}q^2 + 4b_{\infty}^{(1)}$ |
| 3 | 3 | -1 | $\frac{1}{3}s_{\infty}$ | -1 | $\frac{4}{81}$ |
| | 2 | $\frac{5}{2}s_{\infty}$ | $\frac{1}{2}q^2 - \frac{3}{2}s_{\infty}^2 + 6b_{\infty}^{(1)}$ | $\frac{1}{2}s_{\infty}$ | $-\frac{5}{9}s_{\infty}$ |
| | 1 | $\frac{3}{2}q^2 - s_{\infty}^2 + 18b_{\infty}^{(1)}$ | $-\frac{7}{2}q^2 s_{\infty} + s_{\infty}^3$ $-18s_{\infty} b_{\infty}^{(1)} + 6b_{\infty}^{(1)2}$ $-12b_{\infty}^{(2)}$ | $q^2 - 6s_{\infty}^2 + 36b_{\infty}^{(1)}$ | $-\frac{4}{9}q^2 + \frac{2}{3}s_{\infty}^2$ $-\frac{16}{3}b_{\infty}^{(1)}$ |
| | 0 | $-\frac{3}{2}q^2 s_{\infty} - 6s_{\infty} b_{\infty}^{(1)}$ $+3b_{\infty}^{(1)2} - 6b_{\infty}^{(2)}$ | $-\frac{1}{8}q^4 + 3q^2 s_{\infty}^2$ $-15q^2 b_{\infty}^{(1)} + 6s_{\infty}^2 b_{\infty}^{(1)}$ $-36b_{\infty}^{(1)2} - 3s_{\infty} b_{\infty}^{(1)2}$ $+2b_{\infty}^{(1)3} + 6s_{\infty} b_{\infty}^{(2)}$ $-6b_{\infty}^{(1)} b_{\infty}^{(2)} + 6b_{\infty}^{(3)}$ | $-\frac{11}{8}q^2 s_{\infty} + s_{\infty}^3$ $-30s_{\infty} b_{\infty}^{(1)} + 9b_{\infty}^{(1)2}$ $-18b_{\infty}^{(2)}$ | $q^2 s_{\infty} + 4s_{\infty} b_{\infty}^{(1)}$ $-2b_{\infty}^{(1)2} + 4b_{\infty}^{(2)}$ |

Benassi and Grecchi [25] gave the first two terms in Eq. (82) for $|E|$. For $\arg E$, their second term is the same as ours when corrected by a factor of 2. The coefficients $e_p^{(N)}$ for $N \leq 3$ are also listed in Table III.

E. Trajectories for f revisited backwards

It is informative to take another *qualitative* look at the path f follows as F runs from ∞ back towards 0 in the light of the asymptotic formula (76). First fix n_{∞} . Take $n_2 = n_{\infty}$, and let successively $n_1 = n_{\infty} + 1, n_{\infty} + 2, \dots$. This is the case that the f curve ends up on the n_2 triple sheet, which means that β_1 ends up at $-\beta_2(1, 0)$, and that the f trajectory has to pass through the (n_1, n_2) branch cut between the n_1 and n_2 triple sheets. Our aim is to describe how this happens by starting from $F = \infty$.

As F decreases from ∞ , $\arg f$ is given initially by [recall that $v \sim 1/(2 \ln F)$]

$$\begin{aligned} \arg f &\sim -2\pi + [12k + 1]v\pi \\ &\sim -\pi - [12(n_1 - n_2) - 1]v\pi. \end{aligned} \quad (84)$$

As $n_1 - n_2 = -k$ takes on the values 1, 2, \dots , the scaled field f lifts progressively higher into the second quadrant. Refer to Fig. 7(c), for which $n_{\infty} = n_2 = 0$ and $n_1 = 3$. The curve for f for $n_1 = 4$, traversed backwards from the origin on the n_2 triple sheet, will rise faster than the (0,3)

curve, and will “pick off” the next branch point (0,4). For each successively higher n_1 the f trajectory rises faster to pass to the right of the next succeeding branch point. The branch points $f_{n_2, n_2+|k|}^{(2)}$ in the second quadrant lie on a convex upwards arc [compare also Fig. 1(a) for the $f_{n_2, n_1}^{(3)}$], which makes it possible to pick off the branch points in a monotonic manner.

Second take $n_1 = n_{\infty}$, and let successively $n_2 = n_{\infty} + 1, n_{\infty} + 2, \dots$. This is the case that the f curve ends up on the n_1 triple sheet, which means that β_2 ends up at $-\beta_1(1, 0)$ and that the $fe^{-i\pi}$ trajectory has to pass through the (n_1, n_2) branch cut between the n_1 and n_2 triple sheets. As F decreases from ∞ , $\arg(fe^{-i\pi})$ is given initially by

$$\begin{aligned} \arg(fe^{-i\pi}) &\sim -2\pi + [12k + 1]v\pi \\ &\sim -2\pi + [12(n_2 - n_1) + 1]v\pi. \end{aligned} \quad (85)$$

As n_2 increases from n_1 , the trajectory for $fe^{-i\pi}$ rises more strongly in the first quadrant and can pick off the next higher branch point $f_{n_1, n_1+|k|}^{(1)}$. Figure 8(b), with the dashed curve traced counterclockwise, is useful for visualizing this process.

In the view from $F = \infty$, the initial triple sheet is $T_{n_{\infty}}$. Whether the f trajectory or the $fe^{-i\pi}$ trajectory traverses a branch cut—which determines whether $\beta_1(1, f)$ or $\beta_2(1, fe^{-i\pi})$ changes branches—is determined by the

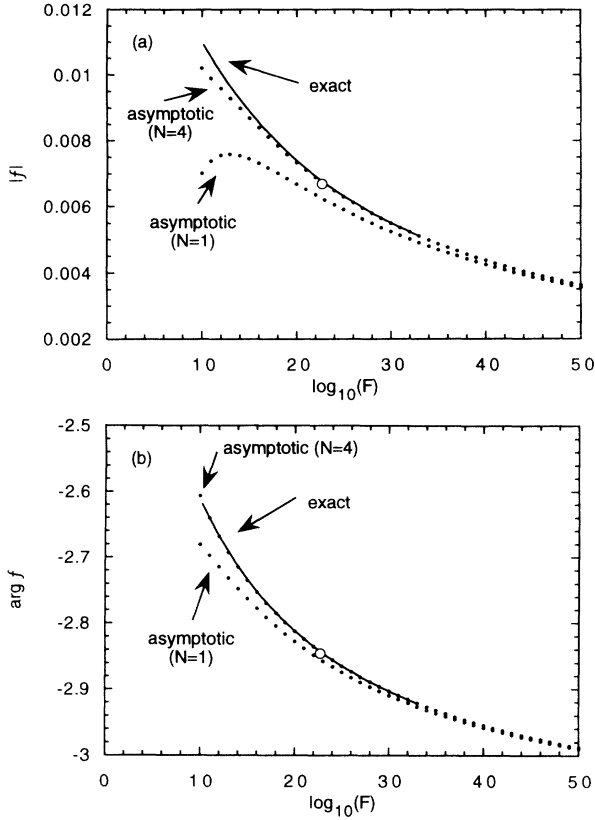


FIG. 9. Scaled field f vs F as given by exact calculation and by asymptotic formulas for the $(0,1,0)$ resonance. Solid line, exact calculation; small open circles, asymptotic formulas (73) and (77) [cf. also Table III] with $N = 1$; filled circles, asymptotic formulas with $N = 4$; large open circle, the highest field calculated by Benassi and Grecchi [25]. (a) $|f|$ vs $\log_{10} F$. (b) $\arg f$ vs $\log_{10} F$.

sign of $k = n_2 - n_1$. If $k < 0$, then consistent with Eq. (84), f passes through the $(n_\infty, n_\infty + |k|)$ branch cut, and $n_1 = n_\infty + |k|$, leaving $n_2 = n_\infty$. If $k > 0$, then consistent with Eq. (85), $f e^{-i\pi}$ passes through the $(n_\infty, n_\infty + k)$ branch cut, and $n_2 = n_\infty + k$, leaving $n_1 = n_\infty$.

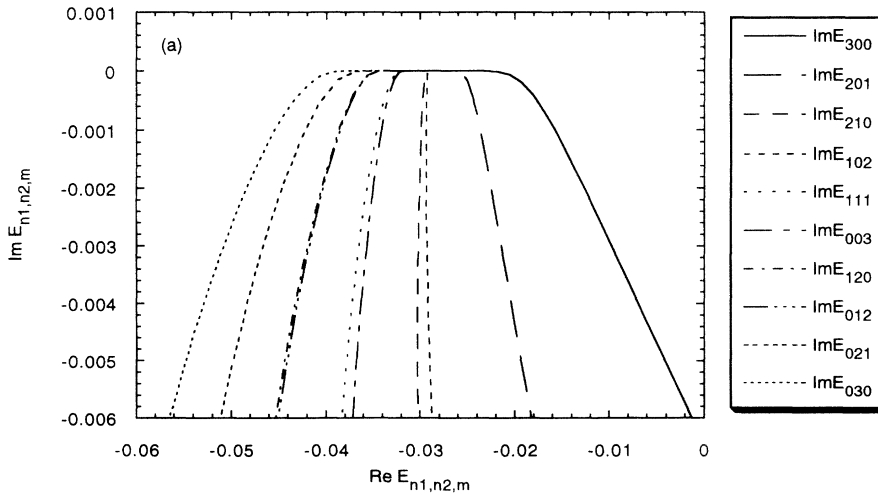


FIG. 10. Trajectories for the complex energy levels of the $n = 4$ resonances. (a) Physical region: $F \leq 5 \times 10^6$ V/cm ~ 0.001 a.u. (b) “Atomic region”: $F \sim 1$ a.u. (c) Unphysically large F : $F \sim 10^{30}$ a.u. (d) Same as (c), except that the asymptotic formulas (80) and (83) with $N = 3$ were used to calculate the energies.

F. Onset of the asymptotic regime for f

When is f given accurately by the asymptotic formula? The answer depends on the quantum numbers of the resonance and is illustrated in Fig. 9 for the excited state calculated by Benassi and Grecchi [25], $(n_1, n_2, m) = (0, 1, 0)$. On the scale of Fig. 9(a), the asymptotic formula (73) with $N = 4$ gives $|f|$ accurately at $F \sim 10^{20}$. For $\arg f$, however, formula (77) with $N = 4$ is already accurate at $F \sim 10^{10}$. The highest-field calculations of Benassi and Grecchi are indicated by large open circles in Figs. 9(a) and 9(b).

G. Trajectories for E

We end this section with pictures of E for three scales of F : physical, atomic, and unphysically large—the last to answer the question, when is E given accurately by the asymptotic formula. The trajectories for all the resonances with $n = 4$ are illustrated in Fig. 10.

The physical region here is arbitrarily defined to include fields up to 0.001 a.u. $\sim 5 \times 10^6$ V/cm. In Fig. 10(a) the trajectories all start on the real axis at $E_{n=4} = -1/32$. As F increases, the energies spread out in a “fan” vs F . However, the real parts of the energies are plotted here vs the imaginary parts, not F . The imaginary parts are initially exponentially small, and the result is that the energies appear to spread out to the left and right while staying on the real axis. When F increases sufficiently for the imaginary parts to be visible, the trajectories quickly descend through the exponential regime and spread out into a $\text{Re } E$ vs $\text{Im } E$ fan pointing downward.

The “atomic” region here is arbitrarily defined to mean that F is approximately 1 a.u. Figure 10(b) shows the same trajectories as in Fig. 10(a), except that the scale is now a.u. rather than hundredths or thousands of an a.u. The spokes of the $\text{Re } E$ vs $\text{Im } E$ fan now look almost like straight lines. Note that in all parts of Fig. 10, three “pairs” of trajectories are grouped naturally by their values of $n_1 - n_2$. The asymptotic expansions are not appropriate for the atomic region because

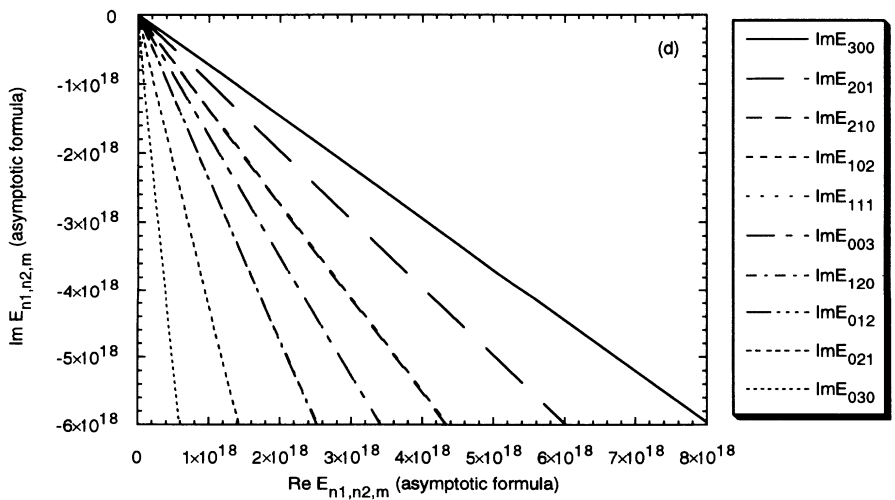
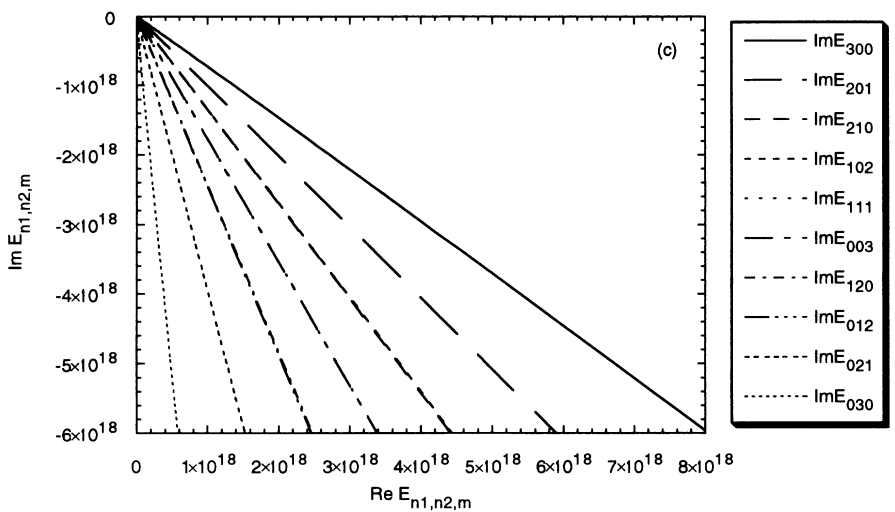
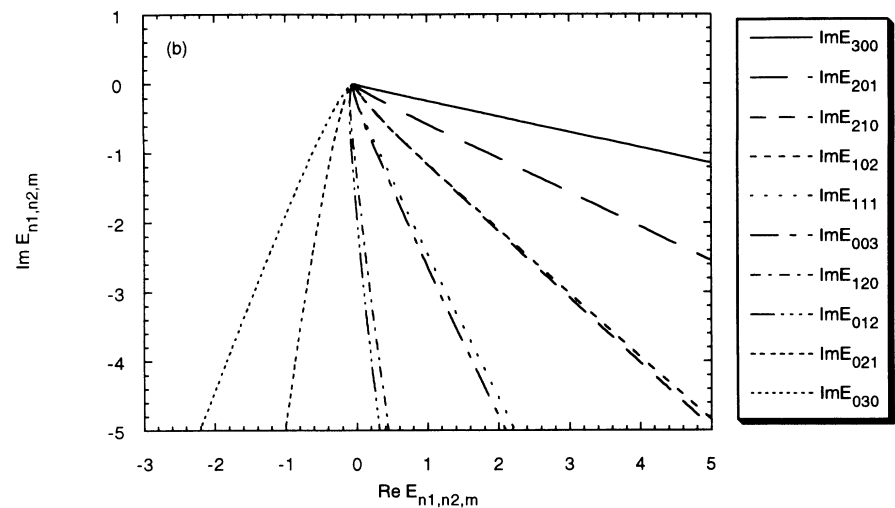


FIG. 10 (Continued).

$F < 4[n_\infty!(n_\infty + m)!]^3$. Thus v would be negative, and w would be the logarithm of a negative number.

In Fig. 10(c) the same trajectories are carried to $F \sim 1 \times 10^{30}$ a.u. Figure 10(d) is the same as Fig. 10(c), except that the asymptotic formulas (80) and (83) with $N = 3$ were used to calculate the energies. On the one hand, it is clear that the asymptotic formulas reproduce the exact calculation very well. On the other hand, the clear implication of Eq. (80) is that all the trajectories should have asymptotic phase $-\pi/3$. Yet the trajectories are substantially spread out in Figs. 10(c) and 10(d). The explanation is simple. The leading term in the deviation from $-\pi/3$ is $-2qv/3$. When $F \sim 10^{30}$, one finds that

$$\arg E + \pi/3 \sim -\frac{2}{3}qv \quad (86)$$

$$\sim -\frac{2}{3}[12(n_2 - n_1) + 1]\pi/(2 \ln F) \quad (87)$$

$$\sim -[12(n_2 - n_1) + 1]\pi/(3 \times 30 \times \ln 10) \quad (88)$$

$$\sim -0.058(n_2 - n_1)\pi, \quad (89)$$

which implies an approximately 60° difference between $\arg E$ for (3,0,0) vs (0,3,0).

VI. SUMMARY

In the LoSurdo-Stark effect, as the electric field $F \rightarrow \infty$, the resonance eigenvalues asymptotically tend to infinity along the ray, $\arg E = -\pi/3$. The leading term of the asymptotic magnitudes (independent of the resonance) is given by

$$|E| \sim \frac{1}{2} \left| \frac{1}{2} F \ln F \right|^{2/3}, \quad (90)$$

while the full expansion is given by Eqs. (53)–(81).

The derivation of the asymptotics is perhaps even more interesting, because it leads to results on the analytic structure of the (radially symmetric two-dimensional) quarticly anharmonic oscillator, whose eigenvalue, equation is equivalent to the separated equations for the LoSurdo-Stark effect in parabolic coordinates. The Riemann surface of the anharmonic oscillator consists of

an infinite number of triple sheets. Each triple sheet is identified with a single unperturbed harmonic oscillator eigenvalue, and every pair of triple sheets is joined by exactly two branch cuts. The structure is richer than that conjectured by Bender and Wu, who initially suggested that only the triple sheets corresponding to adjacent quantum numbers (differing by ± 1 in the present case) were joined together. A FORTRAN computer program, designed to compute resonances at physical field strengths, was used without modification to compute resonances at highly nonphysical field strengths. With a slight alteration to the iteration strategy, the same program efficiently found the exact location of the Bender-Wu branch points, tables of which have been given for $m = 0, 1, \text{ and } 2$.

Because of the simple formula that connects the LoSurdo-Stark energy to the inverse square of the sum of the separation constants, the sum of the separation constants must tend to zero as $F \rightarrow \infty$. We have found numerically that the separation constant β_1 returns either to its unperturbed value $\beta_1^{(0)}$ or to $\beta_2^{(0)}$, the unperturbed value of β_2 , whichever is smaller. At the same time, β_2 tends to the negative of whichever unperturbed eigenvalue is smaller. We understood this numerical behavior by following the trajectory of the complex scaled field f . As the real electric field F increased from 0 to ∞ , in each case that $\beta_1^{(0)}$ and $\beta_2^{(0)}$ were not equal, the trajectory of either f or of $e^{-i\pi}f$ looped around a single branch point and passed through the cut that joined the two ($\beta_1^{(0)}$ and $\beta_2^{(0)}$) Riemann triple sheets. All other branch cuts were avoided. No branch cuts were crossed if $\beta_1^{(0)} = \beta_2^{(0)}$.

We derived the large- F asymptotic expansion for E via the known small- f asymptotic expansion for the discontinuity of the separation constant in the f plane across the negative real axis.

ACKNOWLEDGMENTS

The authors wish to thank the Comunidad Autónoma de Madrid and the Comisión Interministerial de Ciencia y Tecnología for partial support under Grant No. PB 89-0133.

[1] A. LoSurdo, *Atti R. Accad. Lincei* **22**, 664 (1913).
 [2] J. Stark, *Berl. Ber.* **1913**, 932 (1913).
 [3] E. Schrödinger, *Ann. Phys. (Leipzig)* **80**, 437 (1926).
 [4] P. M. Koch, *Phys. Rev. Lett.* **41**, 99 (1978).
 [5] R. J. Damburg and V. V. Kolosov, *J. Phys. B* **9**, 3149 (1976).
 [6] R. J. Damburg and V. V. Kolosov, *J. Phys. B* **11**, 1921 (1978).
 [7] R. J. Damburg and V. V. Kolosov, *J. Phys. B* **12**, 2637 (1979).
 [8] E. Luc-Koenig and A. Bachelier, *J. Phys. B* **13**, 1743 (1980).

[9] E. Luc-Koenig and A. Bachelier, *J. Phys. B* **13**, 1769 (1980).
 [10] H. J. Silverstone, *Phys. Rev. A* **18**, 1853 (1978).
 [11] W. P. Reinhardt, *Int. J. Quantum Chem.* **21**, 133 (1982).
 [12] A. Maquet, S.-I. Chu, and W. P. Reinhardt, *Phys. Rev. A* **27**, 2946 (1983).
 [13] T. Yamabe, A. Tachibana, and H. J. Silverstone, *Phys. Rev. A* **16**, 877 (1977).
 [14] E. Harrell and B. Simon, *Duke Math. J.* **47**, 845 (1980).
 [15] H. J. Silverstone, E. Harrell, and C. Grot, *Phys. Rev. A* **24**, 1925 (1981).
 [16] S. Graffi and V. Grecchi, *Commun. Math. Phys.* **62**, 83

- (1978).
- [17] W. L. Glab and M. N. Nayfeh, *Phys. Rev. A* **31**, 530 (1985).
- [18] W. L. Glab, K. Ng, D. Yao, and M. H. Nayfeh, *Phys. Rev. A* **31**, 3677 (1985).
- [19] H. Rottke and K. H. Welge, *Phys. Rev. A* **33**, 301 (1986).
- [20] T. Bergeman, C. Harvey, K. B. Butterfield, H. C. Bryant, D. A. Clark, P. A. M. Gram, D. MacArthur, M. Davies, J. B. Donahue, J. Dayton, and W. W. Smith, *Phys. Rev. Lett.* **53**, 775 (1984).
- [21] G. Alvarez and H. J. Silverstone, *Phys. Rev. Lett.* **63**, 1364 (1989).
- [22] G. Alvarez, R. J. Damburg, and H. J. Silverstone, *Phys. Rev. A* **44**, 3060 (1991).
- [23] C. A. Nicolaides and S. I. Themelis, *Phys. Rev. A* **45**, 349 (1992).
- [24] L. Benassi, V. Grecchi, E. Harrell, and B. Simon, *Phys. Rev. Lett.* **42**, 704 (1979).
- [25] L. Benassi and V. Grecchi, *J. Phys. B* **13**, 911 (1980).
- [26] C. M. Bender and T. T. Wu, *Phys. Rev.* **184**, 1231 (1969).
- [27] C. M. Bender, H. J. Happ, and B. Svetitsky, *Phys. Rev. D* **9**, 2324 (1974).
- [28] P. E. Shanley, *Phys. Lett. A* **117**, 161 (1986).
- [29] B. Simon, *Ann. Phys. (N.Y.)* **58**, 76 (1970).
- [30] *Handbook of Mathematical Functions*, edited by M. Abramowitz and I. A. Stegun (Dover, New York, 1972).
- [31] I. Herbst, *Commun. Math. Phys.* **64**, 279 (1979).
- [32] S. Graffi, V. Grecchi, and B. Simon, *J. Phys. A* **12**, L193 (1979).